Energy Conversion and Management 245 (2021) 114619

Contents lists available at ScienceDirect

Energy Conversion and Management

journal homepage: www.elsevier.com/locate/enconman

Exergetic, exergoeconomic and exergoenvironmental analyses of a hybrid combined locomotive powering system for rail transportation

Shaimaa Seyam *, Ibrahim Dincer, Martin Agelin-Chaab

Clean Energy Research Laboratory (CERL), Faculty of Engineering and Applied Science, Ontario Tech. University, Oshawa, Ontario, Canada

ARTICLE INFO

Keyword:
Rail Transportation
Fuel cells
Alternative fuels
Exergy
Exergoeconomic analysis
Exergoenvironmental analysis
Hydrogen

ABSTRACT

Alternative and clean powering options are recognized as a crucial step in making rail transportation environmentally-benign, efficient and sustainable. This paper presents the exergetic, exergoeconomic and exergoenvironmental analyses of a new hybrid locomotive powering system, consisting of an internal combustion engine, molten carbonate fuel cell, gas turbine, and absorption refrigeration system. Five alternative fuels are selected and considered with different concentrations, such as natural gas, methanol, ethanol, dimethyl ether, and hydrogen. The entire system achieves a high exergetic efficiency of 83% with a total exergy destruction of 17 MW. The system components have a total levelized capital cost of 32.15 $/h and component-related environmental impact of 86 mPt/h. The entire system has a specific exergy cost and specific environmental impact of 0.10$/GJ and 69.4 mPt/MJ, respectively. It has the total exergoeconomic and environmental impact factors of 3.7% and 0.015%, and the relative cost and environmental impact differences of 21.9% and 19.4%, respectively. The fuel blend of 75% pure natural gas and 25% hydrogen is found to be the most cost effective option with the least environmental impact, compared to other alternative fuel blends.

1. Introduction

The different modes of transportation have increased due to population growth to facilitate the services among cities and the world [1]. The total transportation energy of Canada has been increased by 17% from 2000 to 2018 to 2,717 PJ [2]. The primary fuels that contribute to transportation are gasoline (56%), diesel (28%), and then turbo-fuels (11%). This results in increasing greenhouse gases (GHG) emissions by 27% to 182 Mt CO_2eq from 2000 to 2018 [2].

Many studies have been implemented on locomotive engines. Hogerwaard and Dincer [3] developed the internal combustion engine (ICE) using ammonia-ultra low sulfur diesel (NH_3-ULSD) to contain ammonia decomposition unit to produce hydrogen from ammonia onboard by recovering heat losses. As a result, the performance of the locomotive engine has been slightly improved by 1%, but carbon emissions have significantly been increased by 53%. Also, Zenith et al. [4] studied the potential of electrification of two non-electrified railway lines in Norway and USA using batteries, hydrogen, or hydrogen-battery powering systems. The electrification has improved the overall train efficiency (60–85%) compared to diesel locomotives (25%), but it requires overhead line equipment, which adds significant annual cost. To reduce this cost, hybridization of hydrogen fuel cell and batteries can be used to improve train performance under governmental economic support as occurred in Norway, and paid back by 2030 in USA.

Alternative fuels have been utilized in numerous recent studies. Some of these have focused on a hybrid locomotive engines [5,6] which was comprised of a solid oxide fuel cell (SOFC) and an ammonia organic Rankine cycle (ORC). They used methane in the gas turbine and SOFC and ammonia in ORC. The total power increased from 87.4 to 239.2 kW with energetic and exergetic efficiencies of 74% and 72%, respectively. Also, Kumar et al. [7] studied the feasibility of 90% diesel substitute with methanol in ALCO-251 locomotive engines in Indian Railways. They conducted a simulation and experimental research. They found that the methanol with diesel pilot injection can improve a brake thermal efficiency from 40% to 42% and decrease the nitrogen oxides 60%.

Few studies have conducted exergoeconomic analysis and exergoenvironmental analysis to address engine systems economically and environmentally. Uysal and Keçebaş [8] performed an exergoeconomic analysis on a real gas turbine engine in order to reduce the exergy destruction cost rate of the system. In addition, Chitgar and Emadi [9] applied exergoeconomic analysis on a hybrid SOFC and gas turbine system combined with a desalination and organic flash cycle for a residential building. The obtained costs were 3.4 ¢/kWh for electricity,

* Corresponding author.
E-mail addresses: shaimaa.seyam@ontariotechu.net (S. Seyam), Ibrahim.dincer@ontariotechu.ca (I. Dincer), Martin.Agelin-Chaab@ontariotechu.ca (M. Agelin-Chaab).

https://doi.org/10.1016/j.enconman.2021.114619
Received 1 February 2021; Accepted 5 August 2021
Available online 27 August 2021

Nomenclature

Symbols

A	area [cm^2]
b	specific exergoenvironmental impact [mpt/mj]
$\dot{B}$	exergoenvironmental rate [mpt/h]
c	specific exergoeconomic rate [$/gj]
C	equipment cost [$]
$\dot{C}$	exergoeconomic rate [$/h]
$\dot{E}x$	exergy [kw]
f	relative cost/exergoenvironmental difference
F	Faraday constant [c/mol]
h	specific enthalpy [kj/kg]
i	interest rate [%]
j	current density [ma/cm^2]
N	number of cells/stacks
m	component mass [kg]
$\dot{m}$	mass flow rate [kg/s]
P	pressure [kpa]
$\dot{Q}$	heat rate [kw]
r	exergoeconomic/exergoenvironmental factor
R	resistive loss [$\omega - cm^2$]
$\overline{R}$	molar gas constant [j/mol.k]
s	specific entropy [kj/kg.k]
T	temperature [k]
v	specific volume [m^3/kg]
V	voltage [v]
$\dot{W}$	power [kw]
y	exergy destruction ratio [%]
y^*	irreversibility ratio [%]
$\dot{Y}$	component-related environmental impact [mpt/h]
Z	purchase equipment cost in 2020 [$]
$\dot{Z}$	total investment cost rate [$/h]

Abbreviations

ARS	absorption refrigeration system
BR	catalytic burner
C	compressor
CC	combustion chamber
CRF	capital recovery factor
DME	dimethyl ether
F	alternative fuels
GT	gas turbine cycle
HX	heat exchanger
ICE	internal combustion engine
MCFC	molten carbonate fuel cell
SR	steam reforming
T	turbine
WGS	water gas shift

Subscript

an	anode
b	environmental
ca	cathode
D	destruction
F	fuel
in	inflow
j	component number
ohm	ohmic
out	outflow
P	product
t	total

Greek letters

π	compression ratio
ε	exergetic efficiency [%]
ξ	inverter efficiency [%]
γ	specific heat ratio

37.8 ¢/m^3 for fresh water and 1.7 $/kg for hydrogen. Aghbashlo et al. [10] performed exergoeconomic analysis on a single-cylinder Recardo diesel engine using different biodiesel concentrations (B5) blended with diesel fuel. They found that the pure diesel decreased to the specific exergy cost 48.81 $/MJ for full load compared to 53 $/MJ for 3% emulsified water-biodiesel (B6W3m). However, the fuel blend of B5W3m had high exergetic efficiency of 28% to 33% according to the engine load percentage and higher exergoeconomic factor of 4% and the minimum relative cost difference of 1.6. That showed the fuel blend of B5W3m was exergetically and economically effective fuel. Cavalcanti et al. [11] performed exergoeconomic and exergoenvironmental analysis on different mixtures of biodiesel and diesel in a direct-injection engine of 27 kW. They found that low biodiesel concentration had a slightly higher exergy efficiency of 33% than pure diesel 32%. Also, the exergoeconomic factor was higher for 5% biodiesel (D95B5) of 0.36% than for pure biodiesel (B100) of 0.16%. However, biodiesel had a lower environmental impact of 55.8 mPt/kg than that 240 mPt/kg of diesel. Increasing the biodiesel concentration decreased the environmental impact from 33.7 mPt/MJ to 19.41 mPt/MJ.

Furthermore, the ICE has been combined with cogeneration power plants in different applications. Hoang [12] reviewed a combined diesel engine and organic Rankine cycle (ORC) to utilize wast heat recovery. This combination can reduce fuel consumption by 10% and increase the overall efficiency to 60–90% according to the working fluid of (ORC). Zhang et al. [13] presented a hybrid system of proton membrane fuel cell and an Otto cycle for vehicles. They found that the efficiency and optimum power density varied with respect to the mole fraction of natural gas and the use of PEM increased the efficiency of the Otto cycle. Additionally, Cavalcanti [14] studied a trigeneration system driven by a dual-fuel marine engine using pure diesel and gas-diesel fuels. He performed thermodynamic and exergoenvironmental analysis to investigate the system performance. The diesel engine produces 6.9 MW of electricity, 28 kW of cooling water, and 280 and 590 kW of heating load. The engine performance enhanced for using pure diesel compared to the gas-diesel fuel. However, the dual fuel (gas-diesel) had less electricity environmental impact of 62 mPt/kWh than 72 mPt/kWh of diesel because of pollution formation of chemical reactions. The specific environmental impact of products was 62 mPt/kWh for electric power, 31 mPt/MJ for chilled water, 13 mPt/MJ for heating services.

Some related studies have been conducted for hybrid power plants. Lee et al. [15] developed a hybrid power generation system and performed exergetic and exergoeconomic analysis. The hybrid system comprises solid oxide fuel cell (SOFC) and ICE, and other additional devices such as heat exchangers and blowers. They used liquified natural gas (LNG). The unit exergy cost of LNG was $12.62/GJ. The researchers found that the extensive exergy destruction occurred in the ICE, followed by heat exchangers then SOFC. Also, the SOFC had the highest exergoeconomic factor of 93%. However, the heat exchanger had the lowest exergoeconomic factor of 7%. The ICE and SOFC produced a power of 11.36 kW and 93 kW, respectively. The net power was 101 kW with an overall system efficiency of 62.1% and exergetic efficiency of 57.0%. In addition, the combination of SOFC and turbomachinery improved the thermal efficiency of overall cycle to reach to 65% [16,17].

As presented before, most of the research conducted on locomotive engines focused on thermodynamic analysis for traditional engines using different fuels and injection methods. There are similar studies

appeared, particularly for hybrid locomotive engines. However, the exergoeconomic and exergoenvironmental analyses have not been conducted on hybrid types of powering options for locomotives yet. The novelties of this paper are threefold: (a) The proposed system is an innovative and newly developed one, particularly for clean rail applications, comprising of three powering systems, such as ICE, MCFC and GT which are uniquely integrated and not considered before. (b) The proposed system uniquely deploys natural gas, methanol, ethanol, dimethyl ether and hydrogen with different blending ratio, and hydrogen is the common fuel, instead of traditional fossil fuels. (c) The proposed system is analyzed using three methods: exergetic analysis, exergoeconomic analysis, and exergoenvironmental analysis to investigate the exergy, cost and emission values accordingly, which in this regard comprehensively evaluates it economically and environmentally. The system developed in this paper is a modified version of a previously developed hybrid combined locomotive engine system by the authors [18]. The specific objectives of this study are listed as follows: (i) to model the proposed system exegetically according to fuel and product exergy rates with various alternative fuels and their blends, (ii) to economically investigate the hybrid combined locomotive system using exergoeconomic analysis, (iii) to environmentally investigate the hybrid combined locomotive system using exergoenvironmental analysis, and (iv) to investigate the usage of alternative fuel blends from economic and environmental aspects.

2. System description

A hybrid combined locomotive engine consists of three subsystems: an internal combustion engine (ICE) with a turbocharger compressor (C1) and turbine (T1); a gas turbine (GT) consisting of a compressor (C2), a combustion chamber (CC) and a turbine (T2), and two heat exchangers (HX1 and HX2); a molten carbonate fuel cell (MCFC) combined with a steam reformer and a water gas shift reactors; and an absorption refrigeration system (ARS), as shown in Fig. 1. The ICE is selected to be EMD 16-710-G3 because it is the most popular engine types in rail transportation sectors in the provinces of Ontario and Quebec in Canada. Five fuel blends are used with different mass fractions as mentioned below:

- F1 (75%wt natural gas and 25%wt hydrogen)
- F2 (75%wt methanol and 25%wt hydrogen)
- F3 (60%wt ethanol and 40%wt hydrogen)
- F4 (60%wt DME and 40%wt hydrogen)
- F5 (15%wt natural gas, 40%wt hydrogen, 15%wt methanol, 15%wt ethanol, and 15%wt DME).

This system is a modified version of the hybrid combined locomotive powering system which was simulated using the Aspen Plus to design and evaluate the system thermodynamically by the authors elsewhere [18].

2.1. Locomotive engine

The locomotive engine is internal combustion engine (ICE) which has the characteristics of dual fuel cycle with two-stroke compression ignition, which its specifications are reported in these references [19,20]. The ideal dual cycle comprises of five processes starting from isentropic compression, and followed by heat addition at constant

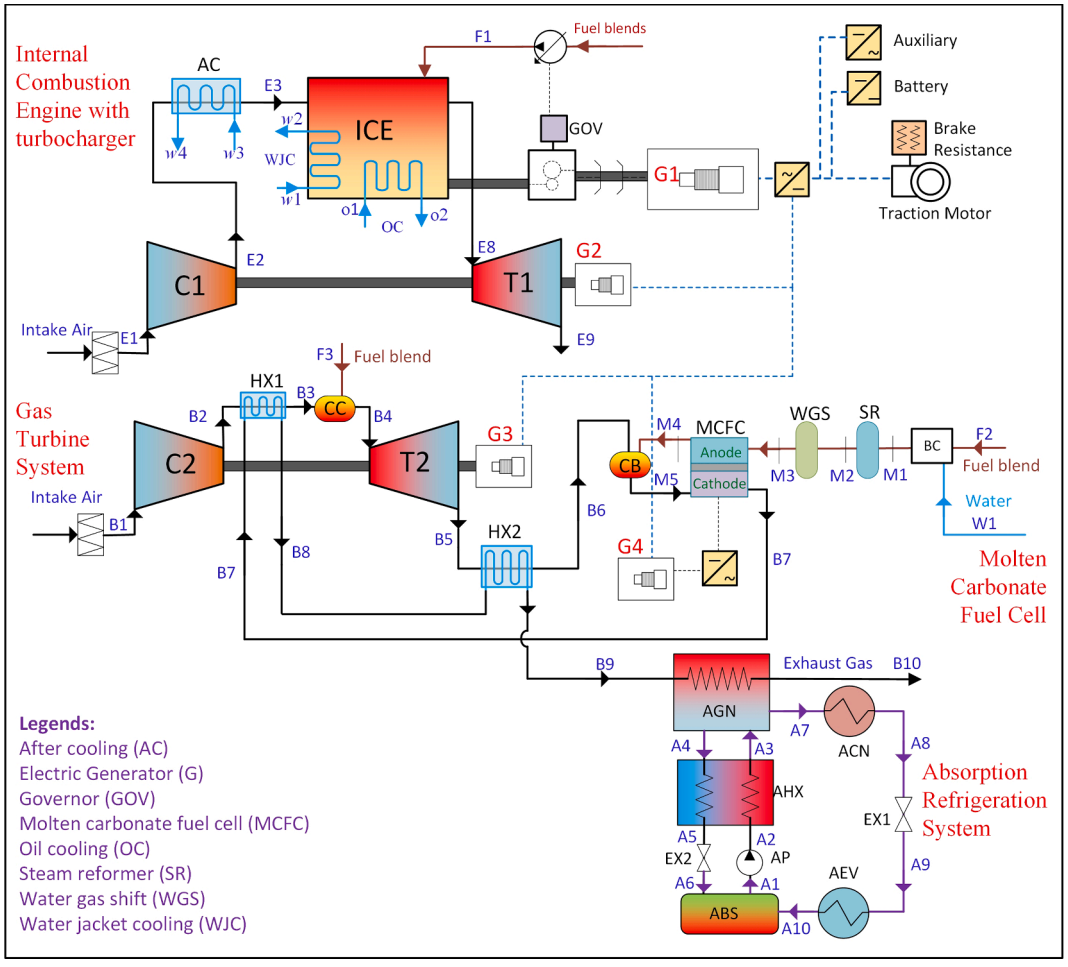

Fig. 1. Configuration of the proposed hybrid combined locomotive system.

volume and heat addition at constant pressure, then isentropic expansion, and finally constant volume heat rejection, as shown in Fig. 2 for T-s diagram. The thermodynamic equations are written for the five processes in Table 1 for the ideal case including the pressure–temperature relationship, and heat and work formulas for each process.

As listed in Table 1, π is the compression ratio ($\pi = 15$), γ is the specific heat ratio of air ($\gamma = 1.4$), v is the specific volume, and c_p and c_v are the specific heat at constant pressure and at constant volume, respectively. The heat addition, $\dot{Q}_A$, to the engine is the total required heat for process 2–4 as, and the heat rejection, $\dot{Q}_R$, is from process 5–1. The engine output power, $\dot{W}_{ICE}$, consists of the net engine power and net power of turbocharger turbine ($\dot{W}_{T1}$) and compressor ($\dot{W}_{C1}$). These parameters are then written as:

$$\dot{Q}_A = \dot{Q}_{2-3} + \dot{Q}_{3-4} \tag{1a}$$

$$\dot{Q}_R = \dot{Q}_{5-1} \tag{1b}$$

$$\dot{W}_{ICE} = \dot{W}_{1-2} + \dot{W}_{3-4} + \dot{W}_{4-5} + \dot{W}_{T1} - \dot{W}_{C1} \tag{1c}$$

For the ICE system, air flows at 3.262 kg/s, 30 °C, and 101.3 kPa and is compressed to 127 kPa into the turbocharger compressor (C1). It then flows at 54.8 °C and 127 kPa to an aftercooled heat exchanger (AC) into the ICE at 25 °C. Also, the fuel blend is pumped at 0.15 kg/s to the ICE for combustion and added work to reach maximum operating condition of 9000 kPa and 1350 °C. Then, the exhaust gas is expanded to 580 °C and 500 kPa and cooled at constant volume at 350 °C and 340 kPa in the ICE. After that, the exhaust gas at 3.412 kg/s is rejected from the engine at a4 and expanded in the turbocharger turbine (T1) to 208 °C and 101.3 kPa at a5. The final exhaust gas is used in the MCFC system. The ICE has a net power of 2570 kW, heat transfer of 7834 kW, a thermal efficiency of 33% and exergy efficiency of 40%, respectively.

2.2. Gas turbine system

The gas turbine (GT) cycle is a reheat-Brayton cycle comprising of a compressor, heat exchanger, combustion chamber, and turbine. The net power, $\dot{W}_{GT}$, and heat combustion, $\dot{Q}_{CC}$, are written below:

$$\dot{W}_{GT} = \dot{W}_{T2} - \dot{W}_{C2} \tag{2a}$$

Table 1
The detailed description of the dual cycle processes.

Process	Description	P-T formulas	Heat	Work
1–2	Isentropic compression	$P_2 = P_1\pi^{\gamma}$ $T_2 = T_1\pi^{(\gamma-1)}$	$\dot{Q}_{1-2} = 0$	$\dot{W}_{1-2} = \dot{m}_a\frac{P_1v_1 - P_2v_2}{(\gamma-1)}$
2–3	Heat addition at constant volume	$\frac{T_3}{T_2} = \frac{P_3}{P_2}$	$\dot{Q}_{2-3} = \dot{m}_{ex}c_v(T_3 - T_2)$	$\dot{W}_{2-3} = 0$
3–4	Heat addition at constant pressure	$\frac{T_4}{T_3} = \frac{v_4}{v_3}$	$\dot{Q}_{3-4} = \dot{m}_{ex}c_p(T_4 - T_3)$	$\dot{W}_{3-4} = \dot{m}_{ex}P_3(v_3 - v_4)$
4–5	Isentropic expansion	$P_5 = P_4\left(\frac{1}{\pi}\right)^{\gamma}$ $T_5 = T_4\left(\frac{1}{\pi}\right)^{(\gamma-1)}$	$\dot{Q}_{4-5} = 0$	$\dot{W}_{4-5} = \dot{m}_{ex}\frac{P_4v_4 - P_5v_5}{(\gamma-1)}$
5–1	Heat rejection at constant volume	$\frac{T_5}{T_1} = \frac{P_5}{P_1}$	$\dot{Q}_{5-1} = \dot{m}_{ex}c_v(T_5 - T_1)$	$\dot{W}_{5-1} = 0$

$$\dot{Q}_{CC} = \dot{m}_{B4}h_{B4} - \dot{m}_F h_{F1} - \dot{m}_{B3}h_{B3} \tag{2b}$$

Note that the air amount at 2.85 kg/s is compressed by (C2) from 101.3 kPa to 1500 kPa, then heated by HX1 from 430 °C to 630 °C. The fuel blend flows at 0.06 kg/s entering the combustion chamber (CC) to heat the air mixture to 980 °C at b3. Then, the air mixture is expanded in the turbine (T2) to 200 kPa in the GT system then used in the MCFC system. The GT net power is 648 kW, and the added heat is 2161 kW. These results show that the performance of GT is 30% and 39% energetic and exergetic efficiency, respectively. The stoichiometric reactions of the fuels that occurred in the combustion chamber and piston chamber are listed below:

- Hydrogen: $2H_2 + O_2 \rightarrow 2H_2O$, $\Delta H_c = -286\,kJ/mol$
- Methanol: $CH_3OH + 1.5O_2 \rightarrow CO_2 + 2H_2O$, $\Delta H_c = -726\,kJ/mol$
- Ethanol: $CH_3OHCH_2 + 3O_2 \rightarrow 2CO_2 + 3H_2O$, $\Delta H_c = -1366.91\,kJ/mol$
- DME: $CH_3OCH_3 + 3O_2 \rightarrow 2CO_2 + 3H_2O$, $\Delta H_c = -2726.3\,kJ/mol$
- NG: $CH_4 + 2O_2 \rightarrow CO_2 + 2H_2O$, $\Delta H_c = -891\,kJ/mol$

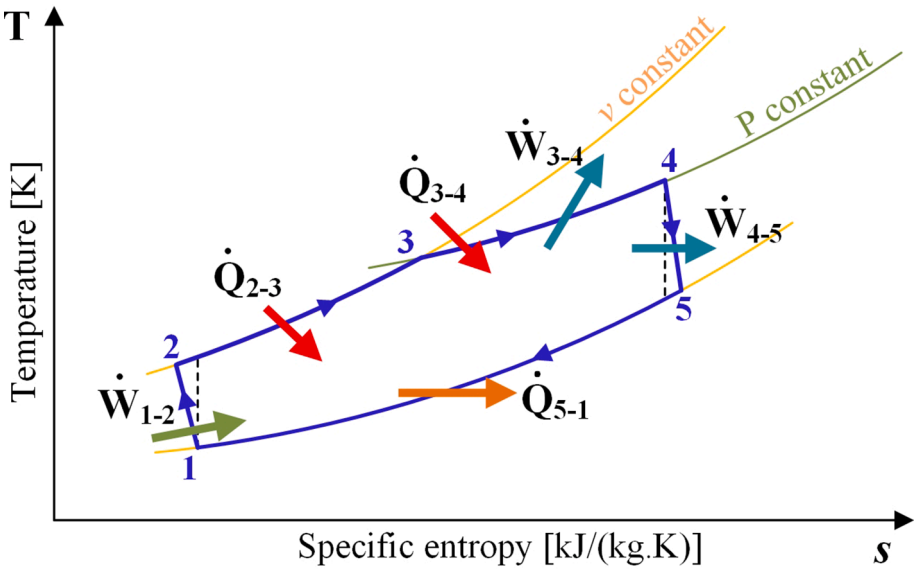

Fig. 2. The T-s diagram of the ICE engine without a turbocharger (Updated from [18]).

2.3. Molten carbonate fuel cell

The molten carbonate fuel cell (MCFC) is manufactured by eutectic mixtures of Li_2CO_3, Na_2CO_3, and K_2CO_3 [21]. The operating temperature should be 923 K (650 °C) greater that the metling point of carbonates (500 °C) preventing electrolyte solidification or volatilization. The specifications of the MCFC are listed in Table 2. The electricity is generated by the electrothermal reactions of the MCFC in the anode and cathode layers as shown below:

- Anode: $H_2 + CO_3^{2-} \leftrightarrow CO_2 + H_2O + 2e^-$
  $CO + CO_3^{2-} \leftrightarrow 2\,CO_2 + 2e^-$
- Cathode: $0.5\,O_2 + CO_2 + 2e^- \leftrightarrow CO_3^{2-}$
- Overall: $H_2 + 0.5\,O_2 + CO_2 \leftrightarrow H_2O + CO_2 \left(\Delta\bar{h}^0_{298K} = -242\,\text{kJ/mol}\right)$

This MCFC system required a steam reforming (SR) and water gas shift (WGS) units placed before the MCFC unit to yield H_2 and CO from the fuel blends in the MCFC stack [22] in the anode layer, which have the chemical reactions as below. However, the CO_2 from WGS is consumed by the electrolyte molten carbonates. Also, any unreacted fuels flow is completely combusted with air in the catalytic burner (BR) and used again in the cathode layer.

- SR: $CH_4 + H_2O \rightarrow CO + 3\,H_2 \quad \Delta\bar{h}^0_{298K} = 206\,\text{kJ/mol}$
- WGS: $CO + H_2O \rightarrow CO_2 + H_2 \quad \Delta\bar{h}^0_{298K} = -41\,\text{kJ/mol}$

The MCFC cell voltage, V_{cell}, is calculated by the reversible potential and reduced by the Nernst loss, concentration loss, and activation polarization [23], which is written as:

$$V_{\text{cell}} = V^0 - V_{Nernst} - j(R_{an} + R_{ca} + R_{ohm}) \tag{3}$$

where V^0 and V_{Nernst} are the reversible voltage at standard conditions and the Nernst voltage loss [V], respectively. Those potentials are maximized at open-circuit conditions there is no current in the circuit. The j is the current density [mA/cm^2]. R_{an}, R_{ca}, and R_{ohm} are the anodic and cathodic activation losses and the ohmic losses [$\Omega-$cm^2], respectively. The activation losses occurs to breakdown the chemical bonds of hydrogen and oxygen molecules in the electrochemical reaction, while the ohmic losses occurs due to the ionic and electronic conduction at the electrodes and the contacts [24]. The detailed equations for each parameter are explained in Eqs. (4)–(8)

$$V^0 = -\frac{\Delta\bar{g}}{nF} \tag{4}$$

$$V_{Nernst} = \frac{\bar{R}T_c}{nF}\ln\left(\frac{P_{H_2,an}P_{CO_2,an}}{P_{H_2,an}\sqrt{P_{O_2,ca}}P_{CO_2,ca}}\right) \tag{5}$$

$$R_{an} = 2.27\times10^{-5}\times\exp\left(\frac{\Delta\bar{h}_{an}}{\bar{R}T_c}\right)\times P_{H_2}^{-0.42}P_{CO_2}^{-0.17}P_{H_2O}^{-1.0} \tag{6}$$

Table 2
The characteristics of MCFC unit.

Elements	Value	Units
Operating temperature, T_c	923	K
Operating pressure, P_c	200	kPa
Current density, j	150	mA/cm^2
Anode activation energy, $\Delta\bar{h}_{an}$	53,500	J/mol
Cathode activation energy, $\Delta\bar{h}_{ca}$	77,300	J/mol
A_c	6700	cm^2
N_c	400 cells	–
N_s	3 stacks	–

Table 3
The chemical reactions of fuel combination in SR, WGS, and CR.

Fuels	SR	WGS	BR
F1	$CH_4 + H_2O \rightarrow CO + 3H_2$	$CO + H_2O \rightarrow CO_2 + H_2$	$CH_4 + 2O_2 \rightarrow CO_2 + 2H_2O$ $2H_2 + O_2 \rightarrow 2H_2O$ $2CO + O_2 \rightarrow 2CO_2$
F2	$CH_3OH \rightarrow CO + 2H_2$	$CO + H_2O \rightarrow CO_2 + H_2$	$CH_3OH + 1.5O_2 \rightarrow CO_2 + 2H_2O$ $2H_2 + O_2 \rightarrow 2H_2O$ $2CO + O_2 \rightarrow 2\,CO_2$
F3	$CH_3OCHH_2 \rightarrow CH_4 + CO + H_2$ $CH_4 + H_2O \rightarrow CO + 3H_2$	$CO + H_2O \rightarrow CO_2 + H_2$	$CH_3OCHH_2 + 3O_2 \rightarrow 2CO_2 + 3H_2O$ $2H_2 + O_2 \rightarrow 2H_2O$ $2CO + O_2 \rightarrow 2CO_2$
F4	$CH_3OCH_3 \rightarrow CH_4 + CO + H_2$ $CH_4 + H_2O \rightarrow CO + 3H_2$	$CO + H_2O \rightarrow CO_2 + H_2$	$CH_3OCH_3 + 3O_2 \rightarrow 2CO_2 + 3H_2O$ $2H_2 + O_2 \rightarrow 2H_2O$ $2CO + O_2 \rightarrow 2\,CO_2$
F5	$CH_4 + H_2O \rightarrow CO + 3H_2$ $CH_3OH \rightarrow CO + 2H_2$ $CH_3OCHH_2 \rightarrow CH_4 + CO + H_2$ $CH_3OCH_3 \rightarrow CH_4 + CO + H_2$	$CO + H_2O \rightarrow CO_2 + H_2$	$CH_4 + 2O_2 \rightarrow CO_2 + 2\,H_2O$ $CH_3OH + 1.5O_2 \rightarrow CO_2 + 2H_2O$ $CH_3OCHH_2 + 3O_2 \rightarrow 2CO_2 + 3H_2O$ $CH_3OCH_3 + 3O_2 \rightarrow 2CO_2 + 3H_2O$ $2H_2 + O_2 \rightarrow 2H_2O$ $2CO + O_2 \rightarrow 2CO_2$

$$R_{ca} = 7.505\times10^{-6}\times\exp\left(\frac{\Delta\bar{h}_{ca}}{\bar{R}T_c}\right)\times P_{O_2}^{-0.43}P_{CO_2}^{-0.09} \tag{7}$$

$$R_{ohm} = 0.5\times\exp\left[3016\left(\frac{1}{T_c}-\frac{1}{923}\right)\right] \tag{8}$$

where F is the Faraday constant (96,485 C/mol), n is the molecular number of H_2, and $\Delta\bar{g}$ is the Gibbs free energy across the fuel cell. $\bar{R}$ is the molar gas constant (8.314 J/molK), and P is the partial pressure at each electrode. $\Delta\bar{h}_{an}$ and $\Delta\bar{h}_{ca}$ are the activation energy values in the anode and cathode, respectively. The net power output of an MCFC [W] is estimated as follows:

$$\dot{W}_{MCFC,AC} = (A_cN_cN_s)\,j\,V_{cell}\,\xi_{DC-AC} \tag{9}$$

where A_c is the active area [cm^2], N_c and N_s are the number of cells per stack and the number of stacks, respectively. ξ_{DC-AC} is the inverter efficiency to flip the direct current (DC) to alternating current (AC) and equals 0.95.

Based on the results of Aspen Plus simulation for MCFC, the fuel flows at 0.05 kg/s is blended with water at 0.1 kg/s. The fuel mixture is heated by the heat exchangers (PR1 and PR2) and enters SR at 300 °C and 200 kPa, then WGS at 400 °C and 200 kPa to enter the MCFC anodic layers at 650 °C and 200 kPa, where the electrochemical reactions happen. Then, the anodic effluent enters a catalytic burner (BR) to combust any by-products with the exhausted air of GT system, where their product flows to the cathodic layer of MCFC to extract the carbon monoxide and carbon dioxide gases by the molten electrolytes. As a result, the exhaust gases has reduced their carbon emissions besides to the electricity generation from the fuel cell. The MCFC system has a net power of 939 kW, heating loss of 565 kW, electric efficiency of 79%, thermal efficiency of 53%, and exergy efficiency of 79%. The chemical reactions fuel combination in the SR, WGS, and CB are tabulated in Table 3.

2.4. Absorption refrigeration system

The absorption refrigeration system (ARS) is used to convert the heating load into the cooling load [25]. The ARS comprises of an

Table 4
Mass balance and energy balance equations for ARS.

Component	Mass Balance	Energy Balance
AGN	$\dot{m}_{A3} = \dot{m}_{A4} + \dot{m}_{A7}$	$\dot{Q}_{AGN} = \dot{m}_{A7}h_{A7} + \dot{m}_{A4}h_{A4} - \dot{m}_{A3}h_{A3}$
ACN	$\dot{m}_{A7} = \dot{m}_{A8}$	$\dot{Q}_{ACN} = \dot{m}_{A8}(h_{A7} - h_{A8})$
AEV	$\dot{m}_{A9} = \dot{m}_{A10}$	$\dot{Q}_{AEV} = \dot{m}_{A9}(h_{A9} - h_{A10})$
ABS	$\dot{m}_{A6} + \dot{m}_{A10} = \dot{m}_{A1}$	$\dot{Q}_{ABS} = \dot{m}_{A6}h_{A6} + \dot{m}_{A10}h_{A10} - \dot{m}_{A1}h_{A1}$
AP	$\dot{m}_{A1} = \dot{m}_{A2}$	$\dot{W}_{AP} = \dot{m}_{A1}(h_{A2} - h_{A1})$
AHX	$\dot{m}_{A2} = \dot{m}_{A3}$ & $\dot{m}_{A4} = \dot{m}_{A5}$	$\dot{Q}_{AHX} = \dot{m}_{A4}(h_{A4} - h_{A5})$

evaporator (AEV), a condenser (ACN), a generator (AGN), an absorber (ABS), a regenerator heat exchanger (AHX), two expansion valves, and a pump (AP). The working fluid is an ammonia-water mixture. Table 4 shows the mass balance and energy balance equations for the ARS components.

For the ARS, the exhaust of MCFC (b7) flows at 6.20 kg/s, and 650 °C and 200 kPa and then is cooled to 575 °C after heating the entrance of combustion chamber, cooled to 534 °C after heating the turbine exit, and cooled to 135 °C after used in ARS. The ARS is operated using an ammonia-water mixture of 5 kg/s, and 10 °C, and 100 kPa at the pump entrance (AP) to be pumped to 2000 kPa. This cooling system uses a heating load of the generator (AGEN) of 3346 kW to provide a cooling load of 615 kW. Therefore, the energetic and exergetic COPs of the ARS are 18% and 10%, respectively.

3. Analysis and assessment

The present paper is primarily focussed on the economic and environmental assessments. These assessments are based on exergetic analysis, which focuses on the second-law thermodynamic analysis and evaluates the irreversibility of the system, and its components. The exergetic analysis is a useful concept and can be associated with costs (so-called exergoeconomic analysis) and environmental impact (so-called exergoenvironmental analysis) to estimate the economic loses and environmental loses due to the irreversibility of the system components. Therefore, exergoeconomic and exergoenvironmental analyses, which are based on exergetic analysis, are conducted to study the performance and hence efficiencies of the hybrid combined engine.

Table 5
The fuel and product exergy for system components.

Component	F-Exergy	P-Exergy
Gas Turbine		
C2	$\dot{E}x^{W}_{C2} = \dot{W}_{C2}$	$\dot{E}x_{B2} - \dot{E}x_{B1}$
HX-1	$\dot{E}x_{B7} - \dot{E}x_{B8}$	$\dot{E}x_{B3} - \dot{E}x_{B2}$
CC	$\dot{E}x_{B3} + \dot{E}x_{F3} + \dot{E}x^{Q}_{CC}$	$\dot{E}x_{B4}$
T2	$\dot{E}x_{B4} - \dot{E}x_{B5}$	$\dot{E}x^{W}_{T2} = \dot{W}_{T2}$
HX-2	$\dot{E}x_{B8} - \dot{E}x_{B9}$	$\dot{E}x_{B6} - \dot{E}x_{B5}$
Fuel Cell		
MX1	$\dot{E}x_{F2} + \dot{E}x_{W1}$	$\dot{E}x_{M1}$
SR	$\dot{E}x_{M1} + \dot{E}x^{Q}_{SR}$	$\dot{E}x_{M2}$
WGS	$\dot{E}x_{M2} + \dot{E}x^{Q}_{WGC}$	$\dot{E}x_{M3}$
MCFC	$\dot{E}x_{M5} - \dot{E}x_{B7}$	$\dot{E}x_{M4} - \dot{E}x_{M3} + \dot{W}_{MCFC} + \dot{E}x^{L}_{MCFC}$
BR	$\dot{E}x_{B6} + \dot{E}x_{E9} + \dot{E}x_{M4} + \dot{E}x^{Q}_{BR}$	$\dot{E}x_{M5}$
ICE Engine		
ICE	$\dot{E}x_{E1} + \dot{E}x_{F1} - \dot{E}x_{E9}$	$\dot{E}x^{W}_{ICE} = \dot{W}_{ICE}$
Absorption refrigeration cycle		
AGN	$\dot{E}x_{B9} - \dot{E}x_{B10} + \dot{E}x_{A3}$	$\dot{E}x_{A7} + \dot{E}x_{A4}$
ACN	$\dot{E}x_{A7} - \dot{E}x_{A8}$	$\dot{E}x^{Q}_{CN}$
AEV	$\dot{E}x^{Q}_{EV}$	$\dot{E}x_{A9} - \dot{E}x_{A10}$
ABS	$\dot{E}x_{A10} + \dot{E}x_{A6}$	$\dot{E}x^{Q}_{AB} + \dot{E}x_{A1}$
AP	$\dot{E}x^{W}_{P} = \dot{W}_{P}$	$\dot{E}x_{A2} - \dot{E}x_{A1}$
AHX	$\dot{E}x_{A4} - \dot{E}x_{A5}$	$\dot{E}x_{A3} - \dot{E}x_{A2}$

The exergetic performance of the locomotive engine is considered in the analysis. The summation of input exergy rates, including the work exergy and thermal exergy, can be described as the fuel exergy rate ($\dot{E}x_{F,j}$), whereas the summation of output exergy rates can be described as the product exergy rate ($\dot{E}x_{P,j}$). The fuel and product exergy rates for the system components are listed in Table 5. The difference between the fuel exergy and product exergy is expressed as the destruction exergy rate, $\dot{E}x_{D,j}$. The irreversibility ratio (y^{*}_{j}) is the ratio of exergy destruction of a component to the total exergy destruction, while the exergy destruction ratio (y_j) is defined as the ratio of exergy destruction to the total fuel exergy rate of the system. The exergetic efficiency of a component (ε_j) is expressed as the ratio of the product to the fuel exergy, whereas for the system (ε_t) is obtained as the ratio of total product exergy rate to the total component exergy rate as follows:

$$\dot{E}x_{D,j} = \dot{E}x_{F,j} - \dot{E}x_{P,j} \tag{10}$$

$$y_j = \frac{\dot{E}x_{D,j}}{\sum \dot{E}x_{F,j}}\ ,\quad y^{*}_{j} = \frac{\dot{E}x_{D,j}}{\sum \dot{E}x_{D,j}}\ ,\quad \varepsilon_j = \frac{\dot{E}x_{P,j}}{\dot{E}x_{F,j}}\ ,\quad \varepsilon_t = \frac{\sum \dot{E}x_{P,j}}{\sum \dot{E}x_{F,j}} \tag{11}$$

3.1. Exergoeconomic analysis

The specific exergy costing SPECO consists of three main steps [26]: identification of exergy streams, the definition of fuel and product, and implementation of cost equations. The exergy costing is defined as the cost rate associated with each exergy stream, including exergy entering and exiting stream matters, exergy power, and thermal exergy rate due to the heat transfer crossing the boundary of the system. Therefore, the cost rate $\dot{C}$ of exergoeconomic analysis of the system can be summarized as follows:

$$\dot{C}_{in} = c_{in}\dot{E}x_{in} \tag{12a}$$

$$\dot{C}_{out} = c_{out}\dot{E}x_{out} \tag{12b}$$

$$\dot{C}_{W} = c_{W}\dot{W} \tag{12c}$$

$$\dot{C}_{Q} = c_{Q}\dot{E}x_{Q} \tag{12d}$$

where $\dot{C}$ is the cost rate used for the exergoeconomic analysis, c denotes the cost per unit of exergy, and $\dot{E}x$ is the associated exergy transfer rate for the stream and the heat transfer. The cost balance can then be written as follows:

$$\sum \dot{C}_{out,j} + \dot{C}_{W,j} = \sum \dot{C}_{in,j} + \dot{C}_{Q,j} + \dot{Z}^{T}_{j} \tag{13}$$

$$\dot{Z}^{T}_{j} = \dot{Z}^{CI}_{j} + \dot{Z}^{OM}_{j} = \dot{Z}^{CI}_{j} \times \varphi = \frac{Z_j \times CRF \times \varphi_{CO}}{\tau} \tag{14}$$

where $\dot{Z}^{T}_{j}$ is the total costs of the capital investment cost ($\dot{Z}^{CI}_{j}$) and operating-maintenance costs ($\dot{Z}^{OM}_{j}$) of each component (j). φ_{CO} refers to the factor of operation-maintenance cost, which is a function of the capital cost. The CRF is the capital recovery factor, which depends on the interest rate and estimated equipment lifetime, and can be estimated using the following equation:

$$\mathrm{CRF} = \frac{i(1+i)^{n}}{(1+i)^{n} - 1} \tag{15}$$

where i, and n denote real interest rate and system lifetime (in years). The i is a function of the nominal interest rate (i_n) and inflation rate (r_f) and can be expressed as $1 + i = (1 + i_n)/(1 + r_f)$. The Z_j the purchase

equipment cost of the component in the year 2020, and it is estimated by the cost equation [27,28] of a component at a reference year and adjusted by the cost index (CEPCI), as follows:

$$Z_j = C_{ref}\frac{\text{CEPCI}_{2020}}{\text{CEPCI}_{\text{ref}}} \tag{16}$$

The number of unknown exergoeconomic costs is greater than the number of exergy cost equations, so it is required to formulate enough auxiliary equations based on the F and P principle of the SPECO method [26]. The F principle refers to the specific exergetic cost linked to the exergy of a fuel stream, which is supplied to the upstream component. Also, the P principle denotes that the specific exergetic cost linked to the exergy unit of the product stream from a component. Therefore, each exiting exergy stream is linked to fuel or a product, and the number of exiting streams (n) equals the total number of fuel streams and product streams. Consequently, the F and P principles offer ($n-1$) auxiliary equations. So, specific exergetic cost of fuel, $c_{F,j}$, specific exergetic cost of a product, $c_{P,j}$, cost rate of exergy destruction, $\dot{C}_{D,j}$, cost rate of exergy loss, $\dot{C}_{L,j}$, and cost rate of a product, $\dot{C}_{P,j}$, are expressed as the following equations:

$$c_{F,j} = \frac{\dot{C}_{F,j}}{\dot{E}x_{F,j}} \tag{17a}$$

$$c_{P,j} = \frac{\dot{C}_{P,j}}{\dot{E}x_{P,j}} \tag{17b}$$

$$\dot{C}_{D,j} = c_{F,j}\dot{E}x_{D,j} \tag{18a}$$

$$\dot{C}_{L,j} = c_{F,j}\dot{E}x_{L,j} \tag{18b}$$

$$\dot{C}_{P,j} = \dot{C}_{F,j} + \dot{Z}_j^T \tag{19}$$

Table 6
The exergoeconomic balance equations for the system components.

Component	Cost Balance Equation	Auxiliary Equations
Gas Turbine		
C2	$\dot{C}_{B1} + \dot{C}_{C2}^W + \dot{Z}_{C1} = \dot{C}_{B2}$	$c_{B1} = 0$
HX-1	$\dot{C}_{B7} - \dot{C}_{B8} + \dot{Z}_{HX1} = \dot{C}_{B3} - \dot{C}_{B2}$	$\frac{\dot{C}_{B2}}{\dot{E}x_{B2}} = \frac{\dot{C}_{B3}}{\dot{E}x_{B3}}$
CC	$\dot{C}_{B3} + \dot{C}_{F3} + \dot{C}_{CC}^Q + \dot{Z}_{CC} = \dot{C}_{B4}$	c_{F3} = fuel cost
T2	$\dot{C}_{B4} - \dot{C}_{B5} + \dot{Z}_{T2} = \dot{C}_{T2}^W$	$c_{B5} = c_{B4}$
HX-2	$\dot{C}_{B8} - \dot{C}_{B9} + \dot{Z}_{HX2} = \dot{C}_{B6} - \dot{C}_{B5}$	$\frac{\dot{C}_{B6}}{\dot{E}x_{B6}} = \frac{\dot{C}_{B5}}{\dot{E}x_{B5}}$
Fuel Cell		
MX1	$\dot{C}_{F2} + \dot{C}_{W1} + \dot{Z}_{MX1} = \dot{C}_{M1}$	$\dot{Z}_{MX1} = 0$, $c_{W1} = 0$
SR	$\dot{C}_{M1} + \dot{C}_{SR}^Q + \dot{Z}_{SR} = \dot{C}_{M2}$	
WGS	$\dot{C}_{M2} + \dot{Z}_{WGS} + \dot{C}_{WGS}^Q = \dot{C}_{M3}$	
MCFC	$\dot{C}_{M5} - \dot{C}_{B7} + \dot{Z}_{MCFC} = \dot{C}_{MCFC}^W + \dot{C}_{M4} - \dot{C}_{M3} + \dot{C}_{MCFC}^L$	$c_{B7} = c_{M4}$
BR	$\dot{C}_{B6} + \dot{C}_{E9} + \dot{C}_{M4} + \dot{Z}_{BR} + \dot{C}_{BR}^Q = \dot{C}_{M5}$	
ICE Engine		
ICE	$\dot{C}_{E1} + \dot{C}_{F1} - \dot{C}_{E9} + \dot{Z}_{ICE} = \dot{C}_{ICE}^W$	c_{F1} = fuel cost, $c_{E1} = 0$
Absorption refrigeration cycle		
AGN	$\dot{C}_{B9} - \dot{C}_{B10} + \dot{C}_{A3} + \dot{Z}_{AGN} = \dot{C}_{A7} + \dot{C}_{A4}$	$c_{A4} = 0$, $c_{B9} = c_{B10}$
ACN	$\dot{C}_{A7} - \dot{C}_{A8} + \dot{Z}_{ACN} = \dot{C}_{CN}^Q$	$c_{A7} = c_{A8}$
AEV	$\dot{C}_{EV}^Q + \dot{Z}_{AEV} = \dot{C}_{A9} - \dot{C}_{A10}$	$c_{A9} = c_{A10}$
ABS	$\dot{C}_{A10} + \dot{C}_{A6} + \dot{Z}_{ABS} = \dot{C}_{A1} + \dot{C}_{AB}^Q$	
AP	$\dot{C}_P^W + \dot{Z}_{AP} = \dot{C}_{A2} - \dot{C}_{A1}$	
AHX	$\dot{C}_{A4} - \dot{C}_{A5} + \dot{Z}_{AHX} = \dot{C}_{A3} - \dot{C}_{A2}$	$c_{A4} = c_{A5}$

where the subscripts P, F, D, and L denote to the exergy product, exergy fuel, exergy destruction, and exergy loss of a component j, respectively. The total specific exergetic cost for fuel ($c_{F,t}$) and for products ($c_{P,t}$) can be defined as:

$$c_{F,t} = \frac{\sum \dot{C}_{F,j}}{\sum \dot{E}x_{F,j}} \tag{20a}$$

$$c_{P,t} = \frac{\sum \dot{C}_{P,j}}{\sum \dot{E}x_{P,j}} \tag{20b}$$

In a particular exergoeconomic evaluation, two parameters are used: the relative cost difference (r_j) and the exergoeconomic factor (f_j). The former refers to the difference between the specific exergetic cost of product and fuel, while the latter refers to the total investment cost rate to the exergy destruction cost rate of a component. They are explained as the followings:

$$r_j = \frac{c_{P,j} - c_{F,j}}{c_{F,j}} = \frac{c_{F,j}\dot{E}x_{D,j} + \dot{Z}_j^T}{c_{F,j}\dot{E}x_{P,j}} \tag{21}$$

$$f_j = \frac{\dot{Z}_j^T}{\dot{Z}_j^T + \dot{C}_{D,j}} = \frac{\dot{Z}_j^T}{\dot{Z}_j^T + c_{F,j}\dot{E}x_{D,j}} \tag{22}$$

The exergoeconomic balance equations are described for each component in the system and listed in Table 6.

3.2. Exergoenvironmental analysis

Exergoenvironmental analysis involves three stages: evaluating exergy of streams through the considered system, performing the life cycle analysis of components and their input streams, and assigning environmental impact from LCA to all streams. This analysis is a proper combination of exergy analysis and LCA since the former analysis assesses the quality of a resource and any thermodynamic inefficiencies, while the latter analysis provides the environmental impacts associated with a component or an overall system during its entire useful life [29].

An environmental impact rate $\dot{B}$ is the environmental impact expressed in points per time unit (Pts/s). It is a weighting method used in the life cycle impact assessment phase to convert the overall environmental impacts of a system to a single value for adequate observability. Therefore, $\dot{B}$ for an entering or exiting stream can be defined as follows:

$$\dot{B}_j = \dot{B}_j^{ch} + \dot{B}_j^{ph} = b_j^{ch}\dot{E}x_j^{ch} + b_j^{ph}\dot{E}x_j^{ph} = b_j\dot{E}x_j \tag{23}$$

where b_j is an environmental impact per unit exergy. The environmental impact rate $\dot{B}_j$ may contain physical and chemical exergy depending on the system or component when a chemical reaction occurs. The environmental impact rates associated with inlet and exit streams, electricity and heat flows may be written respectively as the followings:

$$\dot{B}_{in} = b_{in}\dot{E}x_{in} \tag{24a}$$

$$\dot{B}_{out} = b_{out}\dot{E}x_{out} \tag{24b}$$

$$\dot{B}_W = b_W\dot{W} \tag{24c}$$

$$\dot{B}_Q = b_Q\dot{E}x_Q \tag{24d}$$

The component-related environmental impact is defined as $\dot{Y}_j$, which includes three life cycle phases of construction (including manufacturing, transport, and installation) $\dot{Y}_j^{CO}$, operation and maintenance (including pollutant formation) $\dot{Y}_j^{OM}$ and disposal $\dot{Y}_j^{DI}$, as shown in the following equation:

$$\dot{Y}_j = \dot{Y}_j^{CO} + \dot{Y}_j^{OM} + \dot{Y}_j^{DI} \tag{25}$$

This can be described as $\dot{Y}_j = \left(\dot{Y}_j^{CO} + \dot{Y}_j^{DI}\right)\varphi_{en}$, where φ_{en} refers to the maintenance and operation factor and is equivalent to 1.2. The environmental impact balance equation for each component states that the sum of the environmental impacts associated with the inlet streams plus the component-related environmental impact factor is equal to the environmental impacts associated with the outlet streams, as shown in the following equation:

$$\sum_{k=1}^{m} \dot{B}_{k,j,in} + \dot{Y}_j = \sum_{k=1}^{m} \dot{B}_{k,j,out} \tag{26}$$

The formulated balance equations for all the streams and components are not sufficient to solve for unknown variables. Therefore, auxiliary equations are obtained by applying the *F* and *P* principles from the exergoeconomic analysis, where *F* refers to the exergy fuel while *P* refers to the exergy product for a component (*j*). The exergoenvironmental balance equations are written in Table 7 for each component in the hybrid combined locomotive engine.

In order to account for pollutant formation, a new variable should be defined as $\dot{B}^{PF}$. Pollutant formation terms can be neglected if no pollutants formed within the process, i.e., for a process without a chemical reaction. The value of $\dot{B}^{PF}$, for the components where a chemical reaction occurs, is defined as

Table 7
The exergoenvironmental balance equations for the system components.

Component	Exergoenvironmental Balance Equation	Auxiliary Equations
Gas Turbine		
C2	$\dot{B}_{B1} + \dot{B}_{C2}^{W} + \dot{Y}_{C1} = \dot{B}_{B2}$	$b_{B1} = 0$
HX-1	$\dot{B}_{B7} - \dot{B}_{B8} + \dot{Y}_{HX1} = \dot{B}_{B3} - \dot{B}_{B2}$	$\frac{\dot{B}_{B2}}{\dot{E}x_{B2}} = \frac{\dot{B}_{B3}}{\dot{E}x_{B3}}$
CC	$\dot{B}_{B3} + \dot{B}_{F3} + \dot{B}_{CC}^{Q} + \dot{Y}_{CC} + \dot{B}_{cc}^{PF} = \dot{B}_{B4}$	b_{F3} = fuel impact
T2	$\dot{B}_{B4} - \dot{B}_{B5} + \dot{Y}_{T2} = \dot{B}_{T2}^{W}$	$b_{B5} = b_{B4}$
HX-2	$\dot{B}_{B8} - \dot{B}_{B9} + \dot{B}_{HX2} = \dot{B}_{B6} - \dot{B}_{B5}$	$\frac{\dot{B}_{B6}}{\dot{E}x_{B6}} = \frac{\dot{B}_{B5}}{\dot{E}x_{B5}}$
Fuel Cell		
MX1	$\dot{B}_{F2} + \dot{B}_{W1} + \dot{Y}_{MX1} = \dot{B}_{M1}$	$\dot{Y}_{MX1} = 0$, $b_{W1} = 0$
SR	$\dot{B}_{M1} + \dot{B}_{SR}^{Q} + \dot{Y}_{SR} + \dot{B}_{SR}^{PF} = \dot{B}_{M2}$	
WGS	$\dot{B}_{M2} + \dot{Y}_{WGS} + \dot{B}_{WGS}^{Q} + \dot{B}_{WGS}^{PF} = \dot{B}_{M3}$	
MCFC	$\dot{B}_{M5} - \dot{B}_{B7} + \dot{Y}_{MCFC} + \dot{B}_{MCFC}^{PF} = \dot{B}_{MCFC}^{W} + \dot{B}_{M4} - \dot{B}_{M3} + \dot{B}_{MCFC}^{L}$	$b_{B7} = b_{M4}$
BR	$\dot{B}_{B6} + \dot{B}_{E9} + \dot{B}_{M4} + \dot{Y}_{BR} + \dot{B}_{BR}^{Q} + \dot{B}_{BR}^{PF} = \dot{B}_{M5}$	
ICE Engine		
ICE	$\dot{B}_{E1} + \dot{B}_{F1} - \dot{B}_{E9} + \dot{Y}_{ICE} + \dot{B}_{ICE}^{PF} = \dot{B}_{ICE}^{W}$	b_{F1} = fuel impact, $b_{E1} = 0$
Absorption refrigeration cycle		
AGN	$\dot{B}_{B9} - \dot{B}_{B10} + \dot{B}_{A3} + \dot{Y}_{AGN} = \dot{B}_{A7} + \dot{B}_{A4}$	$b_{A4} = 0$, $b_{B9} = b_{B10}$
ACN	$\dot{B}_{A7} - \dot{B}_{A8} + \dot{Y}_{ACN} = \dot{B}_{CN}^{Q}$	$b_{A7} = b_{A8}$
AEV	$\dot{B}_{EV}^{Q} + \dot{Y}_{AEV} = \dot{B}_{A9} - \dot{B}_{A10}$	$b_{A9} = b_{A10}$
ABS	$\dot{B}_{A10} + \dot{B}_{A6} + \dot{Y}_{ABS} = \dot{B}_{A1} + \dot{B}_{AB}^{Q}$	
AP	$\dot{B}_{P}^{W} + \dot{Y}_{AP} = \dot{B}_{A2} - \dot{B}_{A1}$	
AHX	$\dot{B}_{A4} - \dot{B}_{A5} + \dot{Y}_{AHX} = \dot{B}_{A3} - \dot{B}_{A2}$	$b_{A4} = b_{A5}$

$$\dot{B}^{PF} = \sum_i b_i (m_{out} - m_{in}) \tag{27}$$

where only pollutant streams emitted to the environment are considered, such as CO, CO_2, CH_4, N_2O, NO_x, and SO_x. The average specific environmental impact of fuel (b_{Fj}), product (b_{Pj}), and exergy destruction ($\dot{B}_{Dj}$) for the *j*th component are given as follows:

$$b_{F,j} = \frac{\dot{B}_{F,j}}{\dot{E}x_{F,j}} \tag{28a}$$

$$b_{P,j} = \frac{\dot{B}_{P,j}}{\dot{E}x_{P,j}} \tag{28b}$$

$$\dot{B}_{D,j} = b_{D,j}\dot{E}x_{des,j} \tag{28c}$$

The total specific environmental impact of fuel ($b_{F,t}$), product ($b_{P,t}$) can be descriped as the following:

$$b_{F,t} = \frac{\sum \dot{B}_{F,j}}{\sum \dot{E}x_{F,j}} \tag{29a}$$

$$b_{P,t} = \frac{\sum \dot{B}_{P,j}}{\sum \dot{E}x_{P,j}} \tag{29b}$$

The environmental impact rate balance can be written as:

$$\dot{B}_{P,j} = \sum_{k=1}^{m} \dot{B}_{k,j,in} + (\dot{Y}_j + \dot{B}_j^{PF}) \tag{30}$$

If $\dot{B}^{PF}$ is not considered, the balance equation reduces to $\dot{B}_P = \sum_{k=1}^{m} \dot{B}_{k,j,in} + \dot{Y}_j$. Therefore, the total environmental impact associated with a component, $\dot{B}_{T,j}$, can be given as the following:

$$\dot{B}_{T,j} = \dot{Y}_j + \dot{B}_j^{PF} + \dot{B}_{D,j} \tag{31}$$

To identify the most critical components from the viewpoint of formation of environmental impacts, the sum of environmental impacts $(\dot{Y}_j + \dot{B}_j^{PF} + \dot{B}_{D,j})$ is used. The exergoenvironmental factor f_b is defined as:

$$f_{b,j} = \frac{\dot{Y}_j}{\dot{B}_{T,j}} = \frac{\dot{Y}_j}{\dot{Y}_j + \dot{B}_j^{PF} + \dot{B}_{D,j}} \tag{32}$$

The relative difference of specific environmental impact r_b is an indicator of the potential for reducing the environmental impact associated with a component and is defined as:

$$r_b = \frac{b_{P,j} - b_{F,j}}{b_{F,j}} \tag{33}$$

The specific exergy cost for the fuels, electricity and water are collected from different resources, as shown in Table 8. They are in different units, which have been changed to specific energy cost, $c_{f,en}$ in \$/GJ, and specific exergy cost, $c_{f,ex}$ \$/GJ. The specific exergy cost was estimated as $c_{f,en}$ divided by the exergetic factor of 1.06 [20,21]. The environmental impact b_f is estimated based on three phases of fuels: mining, production, and transportation processes, as shown in Table 5. The life cycle of the fuels is performed using OpenLCA software. The results of the environmental impact for hydrogen and natural gas are compared to that in the TRACI v2.1 [32] and Eco-Indicator database [22,23] to verify the simulation results in the life cycle software. The total cost and environmental impact for the fuel combination are estimated as the summation of mass fraction multiplied by its cost or environmental impact value, as shown in Table 9.

Table 8
The cost and environmental impact of fuels used in this study.

Fuels	Fuel cost	Unit	Ref.	$c_{f,en}$ [$/GJ]	$c_{f,ex}$ [$/GJ]	b_f	Unit	Ref.	b_f [mPt/MJ]
Electricity	0.12	$/kWh	[30]	33.3	31.45	27	mPt/kWh	[34]	
Heating			[30]	2.20	2.08	5.3	mPt/MJ	[34]	5.3
Water				0.10 [a]	0.10	0.026	mPt/kg	[34]	0.012
Air				0[b]	0	0[b]	mPt/kg		0
Hydrogen	2.67	$/kg-$H_2$	[35]	18.82	17.75	731.1[c]	mPt/kg		6.14
Methanol	0.85	$/gal	[36]	8.33	7.86	153.0[c]	mPt/kg		8.45
Ethanol	2.28	$/gal	[37]	25.4	23.96	155.4[c]	mPt/kg		5.82
DME	0.01	$/lit	[38]	149.65	141.18	426.7[c]	mPt/kg		14.78
NG	15.5	$/MWh	[31]	4.31	4.06	260.0[c]	mPt/kg		5.2
$NH_3 + H_2O$	26.5	$/GJ	[39]	26.5	25 [d]	200.0[c]	mPt/kg		10.58
Emissions									
CO_2			[40]		1.54	5.454	mPt/kg	[34]	
CO	0				0	114.6	mPt/kg	[34]	
CH_4	0				0	8.364	mPt/kg	[34]	

[a] assumed value, [b] air is free, [c] estimated using OpenLCA, [d] cost of $NH_3 + H_2O$ at the pump entrance.

Table 9
The composition of fuels, the cost exergy and environmental impact.

Fuels Formulas	NG CH_4	Hydrogen H_2	Methanol CH_3OH	Ethanol CH_3OHCH_3	DME CH_3OCH_3	c_f $/GJ	b_f mPt/MJ
F1	0.75	0.25	0	0	0	7.48	5.44
F2	0	0.25	0.75	0	0	10.33	7.88
F3	0	0.4	0	0.6	0	21.48	5.95
F4	0	0.4	0	0	0.6	91.81	11.33
F5	0.15	0.4	0.15	0.15	0.15	33.66	7.6

4. Results and discussion

The thermodynamic analysis is performed by Aspen Plus simulation for the hybrid combined locomotive engine. This step is necessary to contribute to exergy, exergoeconomic, and exergoenvironmental analysis, as discussed below.

4.1. Exergy analysis results

The exergy flow rates for streams are laid out in the Sankey diagram, including the work and thermal exergy rates for the components, as shown in Fig. 3. The thickness of exergy flow was chosen to be in a scale of 200 kW/1mm. Based on the exergy flow, the ICE has the highest exergy flow, then MCFC, then GT, and lastly ARS. The fuel exergy flow, which is represented in brown colour, of the ICE is the highest (10329

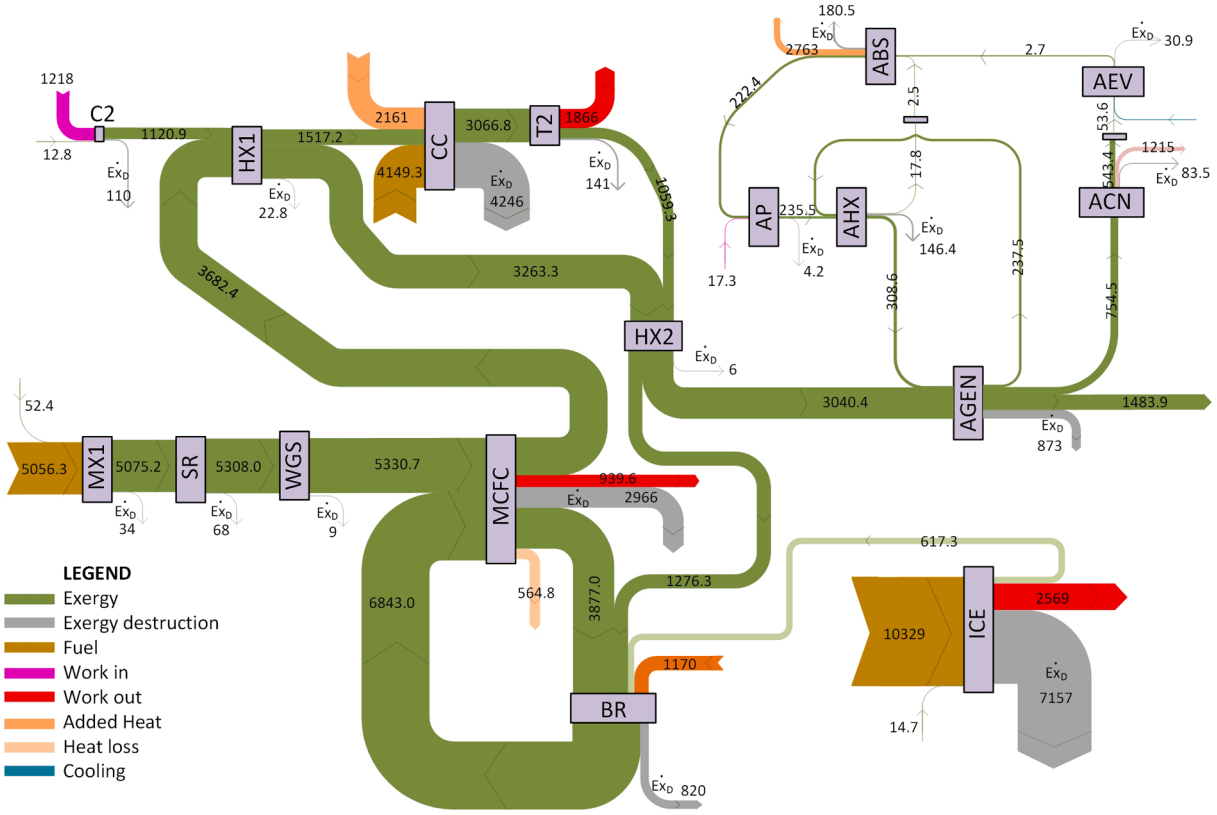

Fig. 3. Sankey Diagram for exergy flow rate in kW.

Table 10
The exergy flow analysis for the components.

Components	$\dot{Q}$ [Kw]	$\dot{W}$ [kW]	$\dot{E}x_F$ [kW]	$\dot{E}x_P$ [kW]	$\dot{E}x_D$ [kW]	$\dot{E}x_L$ [kW]	ε [%]	y [%]	y^* [%]
C2	0	1218	1218	1108	110	0	90.97	0.11	0.65
HX-1	631.8	0	419.1	396.3	22.8	0	94.56	0.02	0.13
CC	2161	0	7313	3067	4246	0	41.94	4.35	25.13
T2	0	1866	2007	1866	141	0	92.97	0.14	0.83
HX-2	348.5	0	223	217	6	0	97.31	0.01	0.04
ICE	0	2569	9726	2569	7157	0	26.41	7.34	42.35
MX1	0	0	5109	5075	34	0	99.33	0.03	0.20
SR	626.4	0	5376	5308	68	0	98.74	0.07	0.40
WGS	58.1	0	5340	5331	9	0	99.83	0.01	0.05
MCFC	564.8	939.6	26,843	23,877	2966	1622	88.95	3.04	17.55
BR	1750	0	31,346	30,526	820	0	97.38	0.84	4.85
AGN	3346	0	1865	992	873	0	53.19	0.89	5.17
ACN	1215	0	211.2	127.7	83.5	0	60.46	0.09	0.49
AEV	615.1	0	81.9	50.95	30.9	0	62.24	0.03	0.18
ABS	2763	0	227.6	47.2	180.5	0	20.72	0.18	1.07
AP	0	17.3	17.26	13.1	4.2	0	75.96	0.00	0.02
AHX	1463	0	219.6	73.2	146.4	0	33.32	0.15	0.87
Total			**97542.6**	**80644.4**	**16898.2**	**1622**	**82.68**	**17.3**	**100**

kW), followed by the MCFC subsystem entiring the mixture at MX1 (5056.3 kW), followed by the combustion chamber (CC) (4149.3 kW). The highest exergy destruction represented in gray is for the ICE, then CC, then MCFC. The thickness of exergy flow increases as the conditions of that flow is far from the standard conditions, and more chemical exergy is added.

In addition, Table 10 presents the heat transfer and power of the components as well as the fuel, product, destruction, and loss exergy flow for each component. The net power of the hybrid combined system is 4139.6 kW, which is estimated as the summation of the net power of gas turbine (648 kW), and the MCFC power (939.6 KW) and the ICE (2569 kW) subtracting the power of pump (17.3 kW). The exergetic efficiency reflects the ratio of exergy product to exergy fuel; as shown in Table 10, the compressor (C2), turbine (T2), heat exchangers (HX-1, HX-2), and reactors (SR, WGS, and BR) have a high exergetic efficiency, more than 90%, while other components like MCFC, ACN, AEV, and AP have moderate exergy efficiency between 60% and less than 90%, and around 50% and below for combustion chamber (CC), absorber (ABS) and generator (AGN). This is due to the high-temperature difference to the standard condition and the high heat of chemical reactions. The total exergetic efficiency, ε_t, is 82.68%. There is another parameter which is used to analyze the system exergetically is y, referring to the ratio of destruction exergy to the total fuel exergy rates. Most of the components have a low y value of less than 1%, whereas the ICE, CC, and MCFC have 7.34%, 4.35%, and 3.04%, respectively. The total destruction ratio, y_t, is 17.3%. The system was operated using F1 (75% NG and 25% H_2).

The current hybrid combined system is compared according to different fuels. Fig. 4 shows the total exergy rates and exergetic efficiency and destruction ratio with respect to fuels. The fuel (F2) has high total exergy fuel and product (107 and 90 MW, respectively) compared to that of F1 (fuel of 97.5 MW and product of 80.6 MW). Note that the minimum fuel and product exergy flow is for F5, about 71 and 54 MW, respectively. The total exergy destruction flow is about 17 MW for all fuels. This yields maximum ε_t and minimum y_t for F2 about 84% and 16%, respectively, whereas F5 has a minimum ε_t and maximum y_t of 76 and 24%, respectively. As presented in Fig. 4, the y_t decreases when ε_t increases because the former counts for the exergy destruction, while the later counts for exergy product. The lower values for exergy fuel and product and higher values of exergy destruction give high value of y_t and low value of ε_t.

4.2. Exergoeconomic analysis results

The exergoeconomic analysis for the hybrid combined locomotive engine is performed. Fig. 4 shows the exergy cost flow rates ($\dot{C}_j$) including the levelized capital cost ($\dot{Z}_k$), which are calculated based on

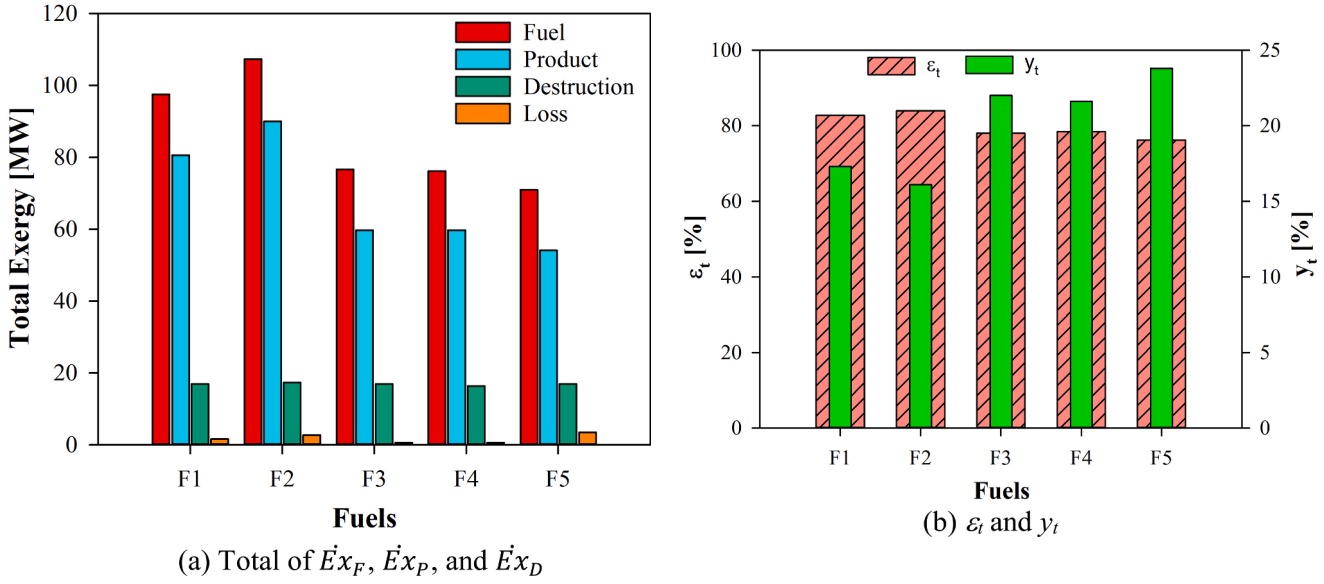

Fig. 4. The total exergy fuel, product, destruction, and loss (a). The total exergy efficiency (ε_t) and total destruction ratio (y_t) (b).

cost equations from Table S-1 (Supplimentary data), power ($\dot{C}_k^W$) and thermal exergetic cost rates ($\dot{C}_k^Q$). Some assumptions are considered to perform the calculations of the exergoeconomic analysis, such as the nominal interest rate is 12%, the lifetime of the engine is 25 years, the annual operation time is 7300 h, the inflation rate is 3%, the maintenance factor is 6%. In Fig. 5, the exergetic cost is drawn at a scale of 10 $/h per 1 mm. The fuel exergy costs are 278.1 $/h for ICE, 136.1 $/h for MX1 entering the MCFC, and 111.7 $.h for CC. The component cost rate ($\dot{Z}_k$) is very small compared to the flow exergy costs of fuel, products, and input and output power. The exergetic cost of the exhaust air to the atmosphere after the generator (AGEN) is estimated to be 185.6 $/h.

Table 11 tabulated the exergoeconomic analysis. The maximum levelized capital cost is for MCFC about 16.52 $/h followed by the ICE (8.29 $/h) then the evaporator AEV (2.00 $/h) then the catalytic burner BR (1.24 $/h). The total levelized capital cost is 32.15 $/h, as shown in Table 8. The total fuel and product exergetic cost rates are 7962.8 and 7992.2 $/h, respectively. The destruction and loss of exergetic cost rates are 847.4 and 12 $/h, respectively. The exergoeconomic factor f for F1 ranges from 0% for the mixer MX1 to 52% for the reactor WGS, while the

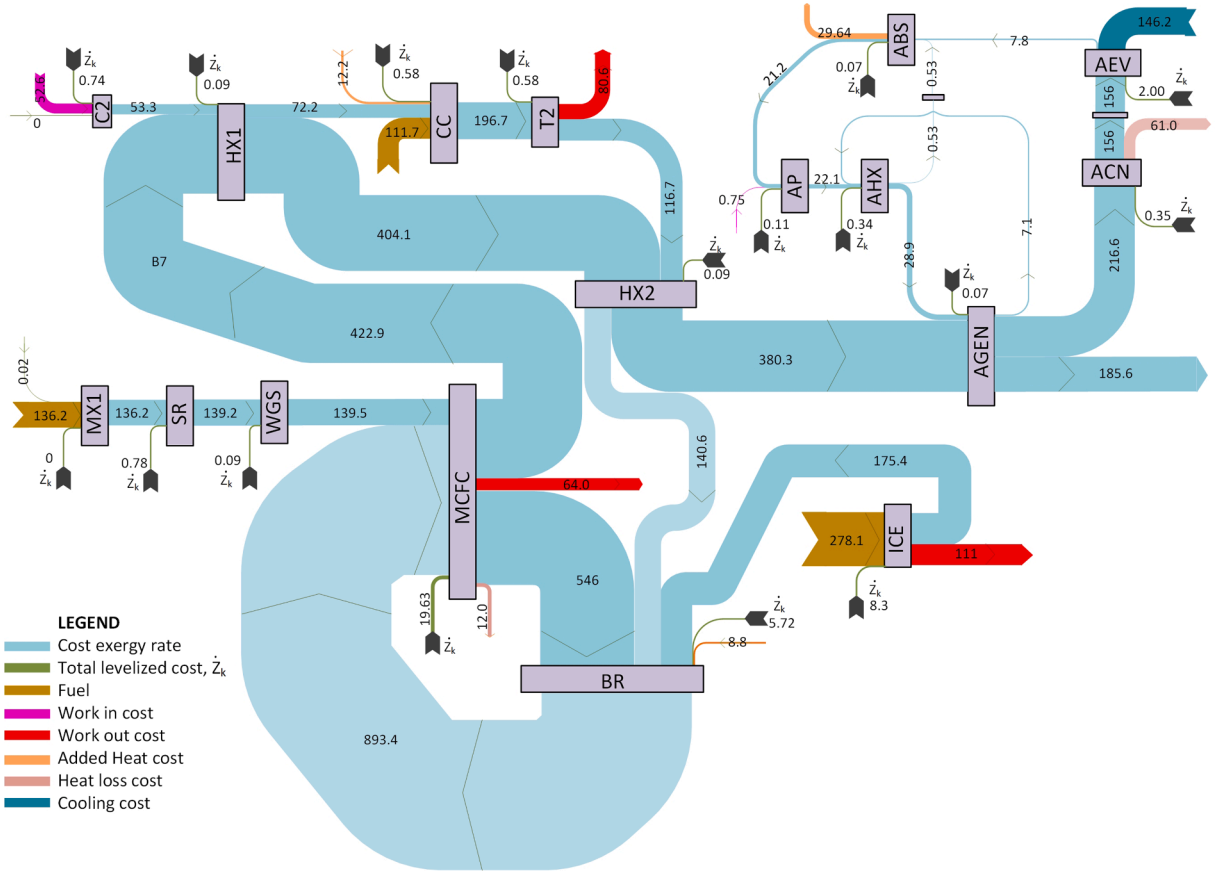

Fig. 5. Sankey diagram for the cost exergy flow rates in [$/h]

Table 11
The results of exergoeconomic analysis of the system components.

Components	$\dot{Z}_k$ [$/h]	$\dot{C}_F$ [$/h]	$\dot{C}_P$ [$/h]	$\dot{C}_D$ [$/h]	$\dot{C}_L$ [$/h]	c_F [$/GJ]	c_P [$/GJ]	f [%]	r [%]
C2	0.74	52.6	53.3	4.8	0.0	12.00	13.37	13.51	11.47
HX-1	0.09	18.8	18.9	1.0	0.0	12.44	13.22	7.96	6.26
CC	0.57	196.1	196.7	113.9	0.0	7.45	17.82	0.50	139.17
T2	0.58	80.0	80.6	5.6	0.0	11.08	12.00	9.32	8.32
HX-2	0.08	23.8	23.9	0.6	0.0	29.67	30.61	11.65	3.15
ICE	8.29	102.7	111.0	75.6	0.0	2.93	12.00	9.89	309.19
MX1	0.00	136.2	136.2	0.9	0.0	7.41	7.45	0.00	0.67
SR	0.86	138.4	139.3	1.8	0.0	7.15	7.29	32.81	1.94
WGS	0.25	139.5	139.7	0.2	0.0	7.26	7.28	51.67	0.31
MCFC	16.52	3100.0	3114.0	342.5	12.0	32.08	36.23	4.60	12.93
BR	1.24	3515.0	3516.0	92.0	0.0	31.15	31.99	1.33	2.72
AGN	0.07	219.8	219.9	102.9	0.0	32.74	61.58	0.06	88.09
ACN	0.35	59.6	59.9	23.6	0.0	78.36	130.34	1.46	66.33
AEV	2.00	143.6	145.6	54.2	0.0	487.29	793.81	3.56	62.91
ABS	0.07	29.4	29.5	23.3	0.0	35.92	173.80	0.30	383.86
AP	0.11	0.7	0.9	0.2	0.0	12.00	18.10	37.77	50.87
AHX	0.34	6.5	6.9	4.3	0.0	8.25	26.03	7.23	215.69
Total	**32.15**	**7962.8**	**7992.2**	**847.4**	**12.0**	**22.68**	**27.53**	**3.66**	**21.89**

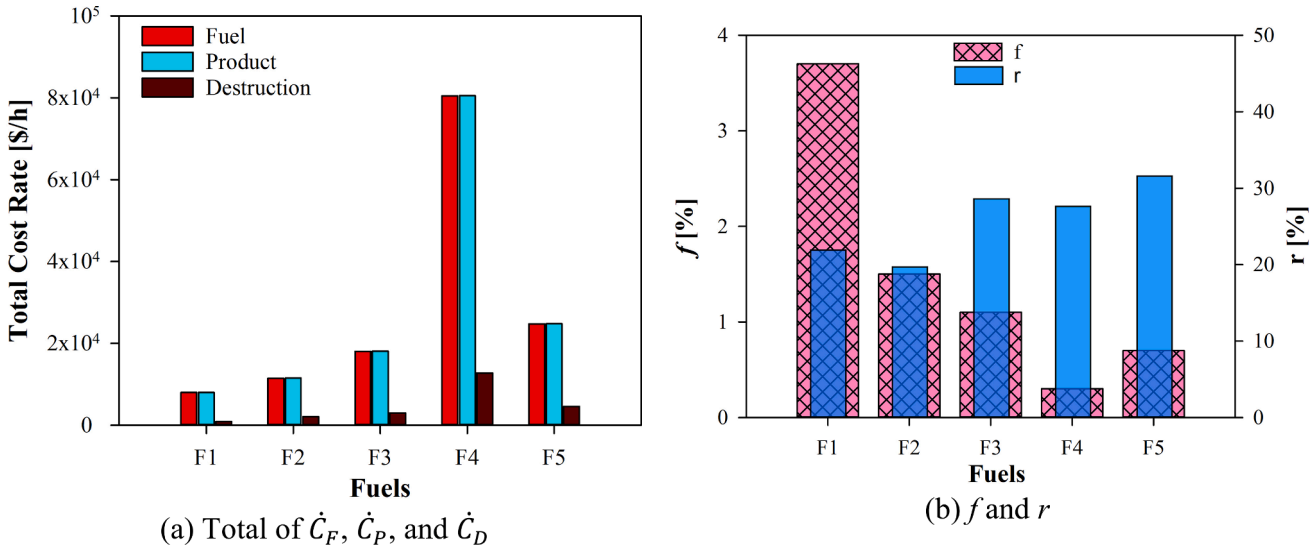

Fig. 6. The total cost rate of exergy fuel $\dot{C}_F$, product $\dot{C}_P$, and destruction $\dot{C}_D$ (a). The total exergoeconomic factor (f) and relative cost difference (r) (b).

relative cost difference r ranges from 0.3% for the water–gas shift to 380% for the absorber in the absorption refrigeration cycle. If the specific exergetic cost for the product c_P is higher than the specific exergetic cost for the fuel c_F multiple times, then the relative cost difference r can be over 100% as calculated for CC (139%), ICE (309%), ABS (384%), and AHX (216%). That is because the product exergy flow rates for those components are less than of the fuel exergy flow rates.

The total exergetic cost for fuel, product, and destruction is compared with respect to fuels F1 to F5, as shown in Fig. 6-a. The exergetic cost rates for fuel and product reach the maximum for F4 (60% DME and 40% H_2) more than 80 K $/h followed by that of F5 (about 25 K $/h), then F3 (18 K $/h $/h), then F2 (11 K $/h), and F1 (8 K $/h). The destruction exergetic cost rate ranges from 850 to 12,000 $/h. This yields to the total exergoeconomic factor, f, is the maximum value of 3.7% for F1 and the minimum value of 0.3% for F4. The total fuel-specific exergetic costs ($c_{F,t}$) are 22.68, 29.72, 65.24, 293.43, 96.87 $/GJ for F1 to F5, respectively. Also, the total product-specific exergetic costs ($c_{P,t}$) are 27.53, 35.48, 83.76, 374.28, 127.30 $/GJ for F1 to F5, respectively. Therefore, the minimum total relative cost difference is 19.7% for F2, as shown in Fig. 5-b, while the maximum total relative cost difference is 31.6% for F5. Therefore, the exergoeconomic factor increases when exergy destruction decreases as well as cost exergy destruction decreases. It is clear that the best economic fuel for the system is pure natural gas, which was assumed as pure methane. In the case that there is no pure natural gas, then the economic fuel is F2, which is a mixture of methanol and hydrogen. In addition, the specific fuel costs mentioned in Table 8 have a significant impact on exergoeconomic analysis since the F1 has less price among them of 7.48 $/GJ. Nowadays, fuel prices are not stable because of COVID-19 holding oil production and businesses. They have a significant impact on the economic analysis.

4.3. Exergoenvironmental analysis results

The exergoenvironmental analysis is performed on the hybrid combined locomotive engine. To estimate the component-related environmental impact $\dot{Y}_j$ that combines the life cycle of construction, operation and maintenance, and disposal. The life cycle of components for construction phase consists of material production and material processing. The operation and maintenance phase is a factor by 1.2 of the construction and disposal phase. The life cycle software used in the analysis is the open LCA, and the environmental impact method is selected to be the Eco-Indicator 99 (EI-99), which is an endpoint environmental impact assessment method of hierarchic perspective employed (it is defined as milipoints per kg [mPt/kg]) and is the summation of normalization of impact categories containing ecosystem quality, human health, and resources [33,34,41]. Table 12 presents the details of material production and the material percentage for each component in the system. The material percentage is assumed based on other literature for the gas turbine cycle [42,43] and estimated based on manufacturing for the fuel cell and absorption refrigeration cycle. The production processing is estimated for each component in Table S-2 (with some supplementary data provided).

Table 13 shows the values of the environmental impact of material production, process, disposal and the total environmental impact as [mPt/kg]. The weights of the components are also listed in Table 13. The total Y is calculated as the total environmental impact multiplied by the component weight. The lifetime of the system is 25 years, and the operation time is 7300 h per year. The weight of the ICE engine is 18,000 kg [44]. The MCFC system, including steam reforming, water gas shift, and catalytic burner, has a weight of 10,336 kg (10 kg/kW [45]). The gas turbine cycle has the least weight of 599 kW [46]. The ABS has a total weight of 4,816 kg (5 ton for 500 kW cooling [25,47,48]). Therefore, the total weight of the hybrid combined locomotive engine is 33,751 kg (~34 ton). The component-related environmental impact rate, $\dot{Y}$, reached the maximum value of 52 mPt/h for ICE, while the values of $\dot{Y}$ for SR, WGS, MCFC, and BR are about 6.9, 3.3, 8.8, and 8.1 mPt/h, respectively. The values of $\dot{Y}$ are dependent on the environmental impact method. However, they can be negligible compared to the environmental impact flow rates of fuel and products [49,50].

The Sankey diagram for exergoenvironmental impact flow rate, $\dot{B}_j$ is illustrated in Fig. 7 and for fuel F1 (75% NG and 25% H_2). The scale of environmental impact flow is 5000 mPt/h per 1 mm. The pollution formation ($\dot{B}^{PF}$) and component-related environmental impact ($\dot{Y}_k$) are included in the figure in gray circle and green arrow, respectively. The fuel exergoenvironmental impact rates are 202,282 mPt/h entering the ICE, 99,022 mPt/h for MX1, and 81,259 mPt/h entering the CC. The exhaust gases for the entire system has an exergoenvironmental rate of

Table 12
The details of material production for each component.

C#	Material	EI-99 [mPt/kg]	Material Percent.	Total EI-99 [mPt/kg]	C#	Material	EI-99 [mPt/kg]	Material Percent.	Total EI-99 [mPt/kg]
C2	Steel	86	33.0	28.4	**ICE**	Steel	86	25	21.5
	Steel LA	110	45.0	49.5		Steel HA	910	22	200.2
	Cast iron	240	22.0	52.8		Aluminum	500	10	50.0
			100	131		Cast iron	240	36	86.4
HX-1	Steel	86	79.4	68.3		Nickel	5200	0.3	15.6
	Steel LA	110	20.6	22.7		Chrome	970	1.7	16.5
			100	91				95	390
CC	Steel	86	33.0	28.4	**MX1**	Steel	86	100	86.0
	Steel HA	910	67.0	609.7	**SR**	Steel HA	910	99	900.9
			100	638		Alumina	1,000	1	10.0
T2	Steel	86	25	21.5				100	911
	Steel HA	110	75	82.5	**WGS**	Steel HA	910	84.000	764.4
			100	104		Alumina	1,000	1.040	10.4
HX-2	Steel	86	79.4	68.3		Cast iron	240	15.090	36.2
	Steel LA	110	20.6	22.7		Nickel	1,200	0.010	0.1
			100	91				100	811
MCFC	Steel	86	80	68.8	**BR**	Steel	86	33.3	28.6
	Steel HA	910	12.07	109.8		steel HA	910	44.5	405.0
	Zinc	3,200	0.4	12.8		Alumina	1,000	22.2	222.0
	Nickel	5,200	0.3	15.6				100	656
	PS	60	0.01	0.0	**AGN**	Steel	86	76	65.4
	Plastics	400	0.03	0.1		Steel LA	110	24	26.4
	Copper	1,400	0.3	4.2				100	92
	MAS	450	0.75	3.4	**ACN**	Steel	86	78	67.1
	Alumina	1000	5.69	56.9		Steel LA	110	22	24.2
	Aluminum	500	0.45	2.3				100	91
			100	274	**AEV**	Steel	86	80	68.8
ABS	Steel	86	80	68.8		Steel LA	110	20	22.0
	Steel LA	110	20	22.0				100	91
			100	91	LA … low alloy				
AP	Steel	86	35	30.1	HL … High alloy				
	Cast iron	240	65	156.0	MAS … microporous alumina-silica				
			100	186	PS … Purified silica				

Table 13
The component-related environmental impact results.

Components	Weight [kg]	Material Production [mPt/kg]	Material Processing [mPt/kg]	Material disposal [mPt/kg]	Total [mPt/kg]	Total Y [mPt]	$\dot{Y}$ [mPt/h]
C2	250.8	131	11.78	24	166.5	41,748.9	0.275
HX-1	67.8	91	12.05	24	127.0	8,610.3	0.057
CC	15	638	20.00	24	682.1	10,231.2	0.067
T2	265.8	104	11.76	24	139.8	37,149.0	0.244
HX-2	12.05	12.05	12.05	24	127.0	347,966.3	2.288
ICE	18,000	390	26.02	24	440.2	7,923,816.0	52.102
MX1	0	86.0	0	24	110.0	0	0
SR	1096	911	20.00	24	954.9	1,046,570.5	6.882
WGS	578	811	20.00	24	855.1	494,268.7	3.250
MCFC	4164	274	22.24	24	320.1	1,333,013.2	8.765
BR	1758	656	20.00	24	699.6	1,229,875.9	8.087
AGN	480	92	12.05	24	127.8	61,349.3	0.403
ACN	1140	91	12.05	24	127.3	145,157.3	0.954
AEV	2076	91	12.05	24	126.9	263,342.7	1.732
ABS	360	91	12.05	24	126.9	45,666.4	0.300
AP	100	186	16.87	24	227.0	22,697.0	0.149
AHX	660	91	12.05	24	127.0	83,816.7	0.551

129,000 mPt/h. In addition, the exergoenvironmental analysis is listed in Table 14. The total component-related environmental impact is 86.10 mPt/h. the total fuel and product environmental impact flowrates are 5,670,758 and 5,598,191 mPt/h, respectively. That means the hybrid combined system reduces the environmental impact. The total destruction environmental impact flowrates, $\dot{B}_D$, is 641,788 mPt/h. The total pollution factor, $\dot{B}^{PF}$, is −65760 mPt/h, which is due to emissions of CO_2, CO, NO_x, and CH_4 to the atmosphere. The specific exergy environment for fuel and product for the entire system are 568.6 and 926.5 mPt/MJ. Therefore, the exergoenvironmental factor, f_b, which is defined as the ratio of the component environmental impact, $\dot{Y}_k$ to the total environmental impact associated with a component, $\dot{B}_T$.

As shown in Table 14, the value of f_b is very small from 0.003% for the absorber to 1.7% for the water–gas shift. The total f_b for the entire locomotive engine is 0.015% which technically shows a negligible

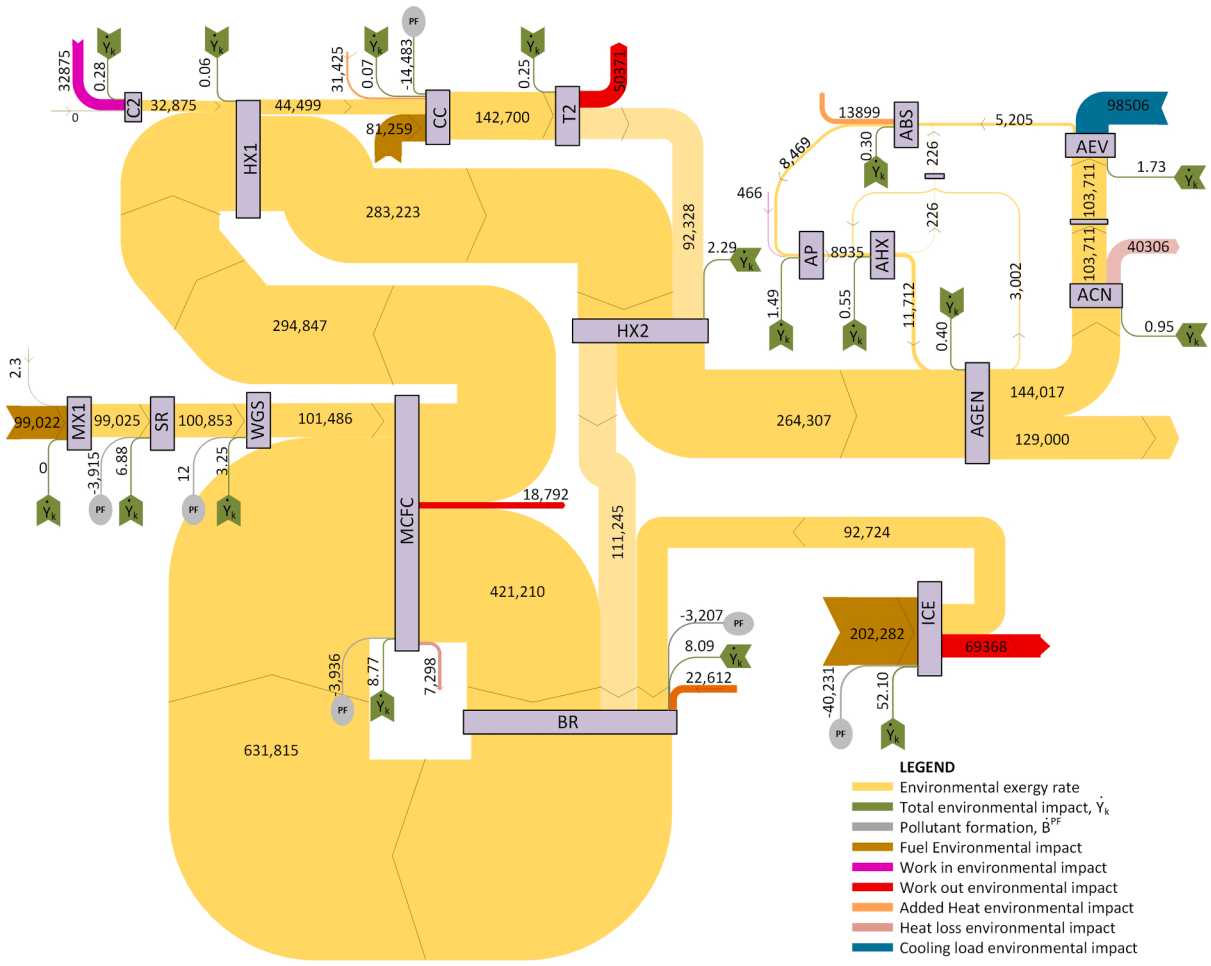

Fig. 7. Sankey diagram for exergoenvironmental impact flow rate for streams [mPt/h].

Table 14
The exergoenvironmental analysis results of the components.

Components	$\dot{Y}$ [mPt/h]	$\dot{B}_F$ [mPt/h]	$\dot{B}_P$ [mPt/h]	$\dot{B}_D$ [mPt/h]	$\dot{B}^{PF}$ [mPt/h]	b_F [mPt/MJ]	b_P [mPt/MJ]	f_b [%]	r_b [%]
C2	0.275	32,875	32,875	3053	0	7.71	8.48	0.009	9.93
HX-1	0.057	11,624	11,624	650	0	7.92	8.38	0.009	5.75
CC	0.067	157,183	142,700	93,869	−14483	6.14	13.29	0.000	116.47
T2	0.244	50,371	50,371	3640	0	7.17	7.71	0.007	7.56
HX-2	2.288	18,916	18,916	524	0	24.24	24.91	0.435	2.76
ICE	52.102	109,558	69,368	82,923	−40231	3.22	7.71	0.122	139.71
MX1	0	99,025	99,025	678	0	5.54	5.57	0	0.67
SR	6.882	104,762	100,853	1363	−3915	5.57	5.43	0.270	2.50
WGS	3.250	101,471	101,486	176	13	5.43	5.44	1.694	0.18
MCFC	8.765	2.19E + 6	2.18E + 6	249,124	−3936	23.33	26.10	0.004	11.86
BR	8.087	2.49E + 6	2.49E + 6	66,999	−3207	22.70	23.28	0.013	2.56
AGN	0.403	147,019	147,019	70,785	0	22.52	42.34	0.0006	88.00
ACN	0.954	40,306	40,306	16,391	0	54.53	90.18	0.006	65.39
AEV	1.732	98,506	98,506	38,258	0	343.81	552.40	0.005	60.67
ABS	0.300	13,899	13,899	11,334	0	17.45	84.22	0.003	382.71
AP	0.149	466	466.1	115	0	7.71	10.16	0.129	31.68
AHX	0.551	2777	2777	1904	0	3.61	10.84	0.029	200.08
Total	**86.10**	**5,670,758**	**5,598,191**	**641,788**	**−65760**	**58.14**	**69.42**	**0.015**	**19.41**

impact of the component-related environmental impact, $\dot{Y}_k$, compared to the destruction, $\dot{B}_D$, and pollution formation, $\dot{B}^{PF}$, of the system components. The relative difference of the specific environmental impact r_b is 63%.

A comparison of the hybrid locomotive engine is considered with respect to different fuels, as displayed in Fig. 7. The total fuel and product exergoenvironmental flow rates are the highest when using fuel F4 (9.15×10^6 and 9.11×10^6 mPt/h, respectively), while the lowest fuel and product exergoenvironmental flow rates are 5.39×10^6 and 5.36×10^6 mPt/h, respectively). The destruction and total environmental impact associated with the entire components have similar values ranging from 0.6×10^6 for F1 to 1.7×10^6 mPt/h for F2, respectively. Fig. 7-b graphs the total values of f_b and r_b, and shows the maximum value of f_b is 0.015% for F1 and the minimum value is 0.005%

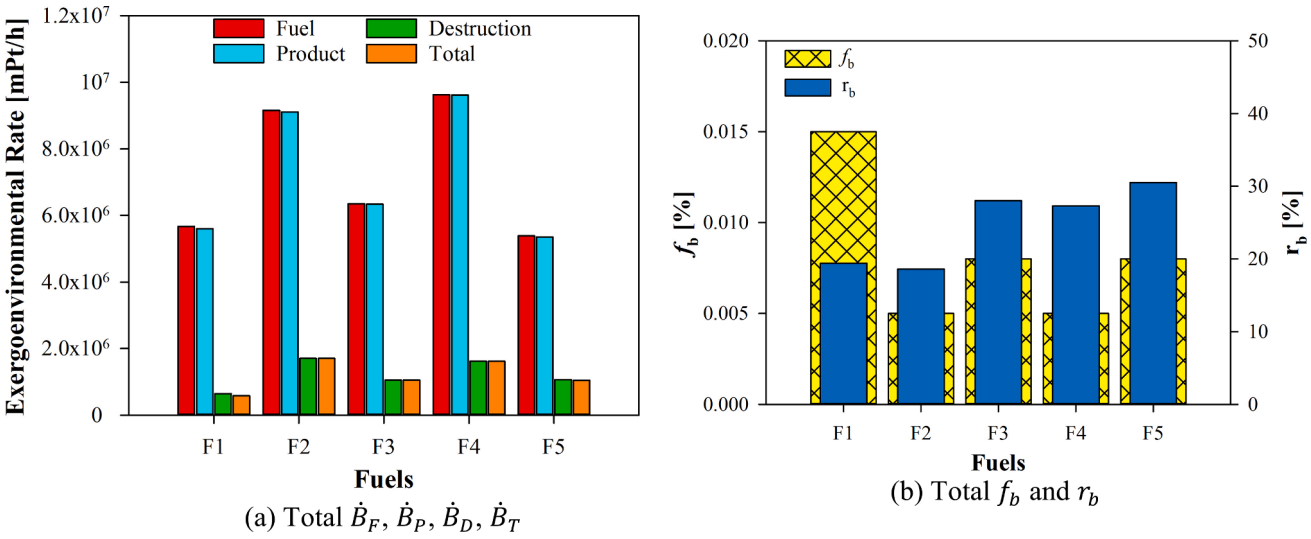

Fig. 8. The total exergoenvironmental impact rate of fuel $\dot{B}_F$, product $\dot{B}_P$, destruction $\dot{B}_D$, and total related to components $\dot{B}_T$ (a). The total exergoenvironmental factor f_b and the relative difference of specific environmental impact r_b (b).

for F2 and F3, while the minimum and maximum values of r_b are 18.6% for F2 and 30.5% for F5. That is because the total specific environmental impact of fuel $b_{F,t}$ is 58.1, 85.3, 82.8, 126.4, and 75.9 mPt/MJ for F1 to F5, respectively, while the total specific environmental impact of product $b_{P,t}$ is 69.4, 101.2, 105.9, 160.9, and 99.0 mPt/MJ for F1 to F5, respectively.

As shown in Fig. 8, lowering exergoenvironmental rates for destruction and pollution formation increases the exergoenvironmental impact factor. Therefore, using a mixture of methane and hydrogen has less environmental impact compared to other fuels by 40%. However, all the fuels have a low environmental impact factor of less than 0.015%, which means all the exergoenvironmental rates of pollution formation and destructions are substantially larger than that related to components. This relationship also reflects on the relative exergoenvironmental impact difference since increasing it means increasing the difference between the exergoenvironmental impact of product and fuel due to increasing environmental impact of destruction and losses. The lower this value, is better and has less impact on the environment.

4.4. Comparison with other systems

The current hybrid combined locomotive system has been compared to three systems as shown in Table 15 for exergoeconomic analysis. The two references have studied hybrid engines. Firstly, Lee et al. [15] studied two systems: SOFC with homogeneous charge compression ignition (HCCI) internal combustion engine and SOFC gas turbine (GT) engine. Both engines were operated using liquefied natural gas (LNG). The fuel specific exergetic cost is 12.05 $/GJ. The specific exergetic cost of electric power produced by fuel cell and HCCI engine are 53.47 and 42.11 $/GJ, respectively. They also used a thermal recovery heat exchanger having a specific exergetic cost of 185.31. The exhaust stream has a specific exrgetic cost of 128.5 $/GJ. Secondly, Marques et al. [51] investigated the exergoeconomic analysis of ICE using natural gas combined with ARS cooling system. the specific exergetic cost of fuel was 17.60 $/GJ. The results of thi system are 29.54 $/GJ for electric power of ICE, 112.01 $/GJ for cooling load, 34.25 $/GJ thermal recovery, and 17.60 $/GJ for exhaust stream.

The current hybrid system consists of four systems as beforementioned (MCFC-GT-ICE-ARS) and operates using five fuels F1 to F5, having specific exergetic costs of 7.48 $/GJ for F1, 10.33 $/GJ for F2, 21.48 $/GJ for F3, 91.81 $/GJ for F4 and 33.66 $/GJ for F5. The electric exergetic costs are constant of 12 $/GJ for ICE and GT, while increasing according to the specific exergetic cost of fuels for electric power of MCFC, thermal recovery, cooling load, and exhaust stream. From this table, we found that the specific exergetic costs for ICE and GT of the current paper achieved minimum values, while the specific exergetic cost of electricity from fuel cell was achieved the minimum for using F1 and F2. The exhaust specific exergetic cost was 34.07 $/GJ for F1 and 49.47 $/GJ for F2, 125.9 $/GJ for F3 and 587.4 $/GJ for F5, which are lower than that of diesel engine alone 529.9 $/GJ. The increase in specific cost of electricity of MCFC results in its high capital cost rate ($\dot{Z}_{MCFC}$) and the increase for the fuel cost for F3, F4 and F5. In addition, the specifc exergetic costs of cooling load are the highest values because of their highest exergy rates for ammonia and water in the evaporator. Furthermore, the increase in specific cost of exhaust stream results in the high values of the total cost rate of components and fuel cost as well.

Limited studies have only conducted an exergoenvironmental analysis on combined systems as for a biodiesel engine [11] and an

Table 15
Comparison the product specific exergetic cost (c_P [$/GJ]) of the current system to other literature.

Ref.	[15]		[51]	Current paper					
System	SOFC-HCCI	SOFC-GT	ICE-ARS	MCFC-GT-ICE-ARS					ICE*
Fuel type	LNG	LNG	NG	F1	F2	F3	F4	F5	Diesel
Fuel input	12.05	12.05	17.60	7.48	10.33	21.48	91.81	33.66	29.01
Electricity by FC	53.47	57.3	0.00	36.23	62.06	155.80	706.24	257.96	0
Electricity by ICE	42.11	0	29.54	12.00	12.00	12.00	12.00	12.00	12
Electricity by GT	0	100.4	0.00	11.08	12.00	12.00	12.00	12.00	0
Thermal recovery	185.31	87.52	34.25	32.74	46.78	111.14	504.34	175.06	0
Cooling	0	0	112.01	793.81	496.30	924.37	4207.72	1490.60	0
Exhaust stream	128.5	52.21	17.60	34.07	49.47	125.9	587.4	200.3	529.9

* only locomotive ICE engine.

Table 16
Comparison of the product specific exergoenvironmental impact (b_P [mPt/MJ]) of the current work.

Fuel type	[11]	[43]	Current paper					
System	ICE	SOFC-GT-ORC	MCFC-GT-ICE-ARS					ICE*
Fuel type	D95B5	NG	F1	F2	F3	F4	F5	Diesel
Fuel input	5.34	3	5.44	7.88	5.95	11.33	7.60	5.54
Electricity by FC	0	1800	26.10	50.72	62.52	83.75	54.38	0
Electricity by ICE	33.7	0	7.71	7.72	7.22	7.71	7.72	7.72
Electricity by GT	0	780	7.71	7.72	7.05	7.71	7.72	0
Thermal recovery	0	0	22.52	37.49	25.17	59.96	36.90	0
Cooling	0	0	343.81	400.49	207.71	497.77	312.46	0
Exhaust stream	22.62	358	24.15	39.80	32.03	66.58	40.17	74.57

* only locomotive ICE engine.

integrated combind system [43]. Cavalcanti et al. [11] studied the impact of using biodiesel fuel of 95% diesel and 5% biodiesel (D95B5) on the environmental impact, as shown in Table 16. The specific exergoenvironmental impact of fuel was 5.34 mPt/MJ resulting the specific exergoenvironmental impact of ICE of 33.7 mPt/MJ and of exhaust stream of 22.62 mPt/MJ. Also, Ghorbani et al. [43] studied an integrated combined system consists of SOFC, GT, and organic Rankine cycle (ORC) using natural gas. The specific exergoenvironmental impact of fuel was 3 mPt/MJ (a conversion of 0.000003Pt/kJ) resulting the specific exergoenvironmental impact of electricity by GT of 780 mPt/MJ, fuel cell (SOFC) of 1800 mPt/MJ and by exhaust stream of 358 mPt/MJ.

For our proposed system, the specific exergoenvironmental impact of fuels are 5.44, 7.88, 5.96, 11.33, and 7.60 mPt/MJ for F1 to F5, respectively, and 5.54 mPt/MJ for diesel fuel. The specific exergoenvironmental impact of electricity for ICE and GT are 7.72 mPt/MJ, while they varies from 26.10 t0 83.75 mPt/MJ for electricity of MCFC. The cooling load has highest environmental impact values. Also, the exhaust streams have specific environmental impact between 24 and 67 mP/MJ. The proposed hybrid-combined locomotive engine has less environmental impact compared to only diesel engine other system as reported in [9,36].

5. Conclusions

This paper presents both exergoeconomic and exergoenvironmental analyses and assessments of a proposed hybrid combined locomotive powering system, which particularly consists of an internal combustion engine, molten carbonate fuel cell with a steam reformer and water–gas shift, gas turbine cycle, and absorption refrigeration system. Based on these detailed analyses and assessments performed, we conclude some remarks as follows:

- The total exergy destruction of the entire system is about 17 MW with 83% exergy efficiency for fuel F1.
- The percentage of exergy destruction to the exergy fuel of the system using natural gas mixture (F1) is 17%.
- The total levelized capital cost is 32.15 $/h, where the MCFC and ICE have the biggest contributions.
- The MCFC and ICE have low exergoeconomic factors of 9.9% and 4.6%, respectively, while the exergoeconomic factor of the system is 3.7% for the F1 fuel (75% NG and 25% H_2).
- The F1 fuel achieves the highest exergoeconomic factor (3.7%) and least relative cost difference (21.9%), which becomes the most cost effective choice because of the least subsidized fuel price.
- The total component-related environmental impact is 86 mPt/h, where the ICE has 52.1 mPt/h.
- The entire system has an exergoenvironmental impact factor for F1 of 0.015% and a relative environmental impact difference of 19.4%. The environmental impact of pollution formation is −65760 mPt/h, which means pollution is removed by the proposed system.
- The specific exergy cost and specific environmental impact of products are 0.1 $/GJ and 69.4 mPt/MJ, respectively.
- The F1 fuel (75% NG and 25% H_2) has the least economic and environmental impact compared to other fuels.

Finally, the key contribution of the proposed hybrid combined locomotive system is to provide a clean rail transportation for the sectors to help improve environmental and economic performances. The integrated system is also considered an ecofriendly approach to produce electric power using alternative fuels for enhancing environmental sustainability and advanced powering systems. With government subsidies, alternative fuels become an economic choice. Further analyses will be performed in the near future with a key focus on multi-objective optimization for improving the economic and environmental impacts of the system.

CRediT authorship contribution statement

Shaimaa Seyam: Conceptualization, Data curation, Formal analysis, Investigation, Methodology, Software, Supervision, Validation, Visualization, Writing - original draft, Writing - review & editing. **Ibrahim Dincer:** Supervision, Conceptualization, Funding acquisition, Writing - review & editing, Project administration, Resources. **Martin Agelin-Chaab:** Supervision, Conceptualization, Funding acquisition, Writing - review & editing, Project administration, Resources.

Declaration of Competing Interest

The authors declare that they have no known competing financial interests or personal relationships that could have appeared to influence the work reported in this paper.

Acknowledgement

The authors acknowledge the financial support provided by the Transport Canada through its Clean Transportation Program-Research and Development and the Natural Sciences and Engineering Research Council of Canada (NSERC).

Appendix A. Supplementary data

Supplementary data to this article can be found online at https://doi.org/10.1016/j.enconman.2021.114619.

References

[1] WorldoMeter. Canada Population (2020). WorldoMeter. <https://www.worldometers.info/world-population/canada-population/>; n.d. (accessed December 25, 2020).
[2] Natural Resources Canada. Energy Fact Book 2020-2021; 2020.
[3] Hogerwaard J, Dincer I. Comparative efficiency and environmental impact assessments of a hydrogen assisted hybrid locomotive. Int J Hydrogen Energy 2016;41(16):6894–904. https://doi.org/10.1016/j.ijhydene.2016.01.118.

[4] Zenith F, Isaac R, Hoffrichter A, Thomassen MS, Møller-Holst S. Techno-economic analysis of freight railway electrification by overhead line, hydrogen and batteries: Case studies in Norway and USA. Proc Inst Mech Eng Part F J Rail Rapid Transit 2020;234(7):791–802. https://doi.org/10.1177/0954409719867495.

[5] Al-Hamed KHM, Dincer I. Investigation of an integrated powering system for clean locomotives with solid-oxide fuel cell with heat recovery organic Rankine cycle. Energy Convers Manag 2020;219:112857. https://doi.org/10.1016/j.enconman.2020.112857.

[6] Al-Hamed KHM, Dincer I. Comparative evaluation of fuel cell based powering systems for cleaner locomotives. Therm Sci Eng Prog 2021;23:100912. https://doi.org/10.1016/j.tsep.2021.100912.

[7] Kumar D, Valera H, Gautam A, Agarwal AK. Simulations of methanol fueled locomotive engine using high pressure co-axial direct injection system. Fuel 2021;295:120231. https://doi.org/10.1016/j.fuel.2021.120231.

[8] Uysal C, Keçebaş A. Advanced exergoeconomic analysis with using modified productive structure analysis: an application for a real gas turbine cycle. Energy 2021;223. https://doi.org/10.1016/j.energy.2021.120085.

[9] Chitgar N, Emadi MA. Development and exergoeconomic evaluation of a SOFC-GT driven multi-generation system to supply residential demands: electricity, fresh water and hydrogen. Int J Hydrogen Energy 2021;46(34):17932–54. https://doi.org/10.1016/j.ijhydene.2021.02.191.

[10] Aghbashlo M, Tabatabaei M, Khalife E, Roodbar Shojaei T, Dadak A. Exergoeconomic analysis of a DI diesel engine fueled with diesel/biodiesel (B5) emulsions containing aqueous nano cerium oxide. Energy 2018;149:967–78. https://doi.org/10.1016/j.energy.2018.02.082.

[11] Cavalcanti EJC, Carvalho M, Ochoa AAV. Exergoeconomic and exergoenvironmental comparison of diesel-biodiesel blends in a direct injection engine at variable loads. Energy Convers Manag 2019;183:450–61. https://doi.org/10.1016/j.enconman.2018.12.113.

[12] Hoang AT. Waste heat recovery from diesel engines based on Organic Rankine Cycle. Appl Energy 2018;231:138–66. https://doi.org/10.1016/j.apenergy.2018.09.022.

[13] Zhang X, Ni M, He W, Dong F. Theoretical analysis and optimum integration strategy of the PEM fuel cell and internal combustion engine hybrid system for vehicle applications. Int J Energy Res 2015;(39). https://doi.org/10.1002/er.3369.

[14] Cavalcanti EJC. Energy, exergy and exergoenvironmental analyses on gas-diesel fuel marine engine used for trigeneration system. Appl Therm Eng 2020:116211. https://doi.org/10.1016/j.applthermaleng.2020.116211.

[15] Lee YD, Ahn KY, Morosuk T, Tsatsaronis G. Exergetic and exergoeconomic evaluation of an SOFC-Engine hybrid power generation system. Energy 2018;145:810–22. https://doi.org/10.1016/j.energy.2017.12.102.

[16] Kumar P, Singh O. Thermoeconomic analysis of SOFC-GT-VARS-ORC combined power and cooling system. Int J Hydrogen Energy 2019;44(50):27575–86. https://doi.org/10.1016/j.ijhydene.2019.08.198.

[17] Liu Y, Han J, You H. Performance analysis of a CCHP system based on SOFC/GT/CO2 cycle and ORC with LNG cold energy utilization. Int J Hydrogen Energy 2019;44(56):29700–10. https://doi.org/10.1016/j.ijhydene.2019.02.201.

[18] Seyam S, Dincer I, Agelin-Chaab M. Development and assessment of a cleaner locomotive powering system with alternative fuels. Fuel 2021;185:120529. https://doi.org/10.1016/j.applthermaleng.2020.116432.

[19] Progress Rail: 710 series engines. Prog Rail. <http://s7d2.scene7.com/is/content/Caterpillar/CM20170915-60253-59723>; n.d. (accessed January 8, 2020).

[20] EMD 710 diesel engine manual, specs and bolt torques. <https://www.barringtondieselclub.co.za/emd/emd-710.html>; n.d. (accessed January 9, 2020).

[21] Li ZL, Devianto H, Kwon H-H, Yoon SP, Lim T-H, Lee H-I. The catalytic performance of Ni/MgSiO3 catalyst for methane steam reforming in operation of direct internal reforming MCFC. J Ind Eng Chem 2010;16(3):485–9. https://doi.org/10.1016/j.jiec.2010.01.058.

[22] Sundmacher K, Kienle A, Pesch HJ, Berndt JF, Huppmann G. In: Molten carbonate fuel cells: modeling, analysis, simulation, and control. Verlag, Wienheim, Germany: Wiley; 2007. https://doi.org/10.1002/9783527611324.

[23] Ahn J, Park SH, Lee S, Noh Y, Chang D. Molten carbonate fuel cell (MCFC)-based hybrid propulsion systems for a liquefied hydrogen tanker. Int J Hydrogen Energy 2018;43(15):7525–37. https://doi.org/10.1016/j.ijhydene.2018.03.015.

[24] Koh J-H, Kang BS, Lim HC. Analysis of temperature and pressure fields in molten carbonate fuel cell stacks. AIChE J 2001;47(9):1941–56. https://doi.org/10.1002/aic.690470906.

[25] Seyam S. Energy and exergy analysis of refrigeration systems. Low-temperature Technol., IntechOpen 2019:13. https://doi.org/10.5772/57353.

[26] Lazzaretto A, Tsatsaronis G. SPECO: A systematic and general methodology for calculating efficiencies and costs in thermal systems. Energy 2006;31(8-9):1257–89. https://doi.org/10.1016/j.energy.2005.03.011.

[27] Turton R, Shaeiwitz JA, Bhattacharyya D, Whiting WB. Analysis, synthesis, and design of chemical processes. 5th ed. Pearson Education, Inc.; 2018.

[28] Aji SS, Kim YS, Ahn KY, Lee YD. Life-cycle cost minimization of gas turbine power cycles for distributed power generation using sequential quadratic programming method. Energies 2018;11(12):3511. https://doi.org/10.3390/en11123511.

[29] Meyer L, Tsatsaronis G, Buchgeister J, Schebek L. Exergoenvironmental analysis for evaluation of the environmental impact of energy conversion systems. Energy 2009;34(1):75–89. https://doi.org/10.1016/j.energy.2008.07.018.

[30] Sönnichsen N. Industrial electricity prices in major Canadian cities 2018. Statista 2020:Energy & Environmental Services/Electricity. <https://www.statista.com/statistics/579159/average-industrial-electricity-prices-canada-by-major-city/> (accessed September 22, 2020).

[31] Tiseo I. Natural gas prices for industry globally by select country 2018. Statista 2020. <https://www.statista.com/statistics/253047/natural-gas-prices-in-selected-countries/> (accessed September 22, 2020).

[32] Hischier R, Weidema B, Althaus H-J, Bauer C, Doka G, Dones R, et al. Implementation of Life Cycle Impact Assessment Methods Data v2.2 (2010). Ecoinvent Rep No 3 2010:176.

[33] Goedkoop M, Spriensma R. The Eco-indicator 99 - A damage oriented method for Life Cycle Impact Assessment; 2001.

[34] Baayen H. In: The Eco-indicator 99: Manual for Designes; 2000. https://doi.org/10.1016/S1359-6462(99)00348-6.

[35] Collins L. "Green hydrogen" on sale in open market at 80% higher price than grey H2 | Recharge. Recharg News. <https://www.rechargenews.com/transition/green-hydrogen-on-sale-in-open-market-at-80-higher-price-than-grey-h2/2-1-743348>; 2020 (accessed September 24, 2020).

[36] Pricing | Methanex Corporation. Methanex Power Agil. <https://www.methanex.com/our-business/pricing>; n.d. (accessed September 22, 2020).

[37] US Departament of Energy. Alternative Fuel Price Report. US DOE Clean Cities. <https://afdc.energy.gov/files/u/publication/alternative_fuel_price_report_april_2020.pdf>; 2020.

[38] ChemBioPower. Using Dimethyl Ether as Fuel for heat, Transportation and Electricity. AZO CleanTech. <https://www.azocleantech.com/article.aspx?ArticleID=713>; 2018 (accessed September 23, 2020).

[39] Zare V, Mahmoudi SMS, Yari M, Amidpour M. Thermoeconomic analysis and optimization of an ammonia-water power/cooling cogeneration cycle. Energy 2012;47(1):271–83. https://doi.org/10.1016/j.energy.2012.09.002.

[40] Government of Canada. Fuel Consumption Levies in Canada. Nat Resour Canada: Transportation fuel prices. <https://www.nrcan.gc.ca/our-natural-resources/domestic-international-markets/transportation-fuel-prices/fuel-consumption-levies-canada/18885?wbdisable=true>; 2020 (accessed September 24, 2020).

[41] Guinée JB. Handbook on life cycle assessment: operational guide to the ISO standards. New York, Boston, Dordrecht, London, Moscow: Kluwer Academic Publishers; 2004.

[42] Boyano A, Blanco-Marigorta AM, Morosuk T, Tsatsaronis G. Exergoenvironmental analysis of a steam methane reforming process for hydrogen production. Energy 2011;36(4):2202–14. https://doi.org/10.1016/j.energy.2010.05.020.

[43] Ghorbani Sh, Khoshgoftar-Manesh MH, Nourpour M, Blanco-Marigorta AM. Exergoeconomic and exergoenvironmental analyses of an integrated SOFC-GT-ORC hybrid system. Energy 2020;206:118151. https://doi.org/10.1016/j.energy.2020.118151.

[44] Progress Rail. EMD 710 series engine benefits Engines 710; n.d.

[45] Vielstich W, Lamm A, Gasteiger HA. In: Handbook of fuel cells - fundamentals, technology and applications. John Wiley & Sons, Ltd; 2010. https://doi.org/10.1002/9780470974001.f500032.

[46] Kerrebrock JL. In: Aircraft engines and gas turbines.. 2nd ed. Massachusetts, USA: The MIT Press; 2012. https://doi.org/10.1007/978-0-230-35686-3_1.

[47] Arora CP. Refrigeration and air conditioning. third ed. New Delhi: Tata McGraw-Hill Publishing Company Limited; 2009.

[48] Ben JR, Ben IN, Ben IS, Bellagi A. Exergy analysis of a diffusion absorption refrigeration system. Int J Exergy 2008;5:626–37. https://doi.org/10.1504/IJEX.2008.020829.

[49] Morosuk T, Tsatsaronis G, Koroneos C. On the Effect of Eco-indicator selection on the conclusions obtained from an exergoenvironmental analysis. Proc. ECOS 2012:1–13.

[50] Morosuk T, Tsatsaronis G, Koroneos C. Environmental impact reduction using exergy-based methods. J Clean Prod 2016;118:118–23. https://doi.org/10.1016/j.jclepro.2016.01.064.

[51] Marques AdS, Carvalho M, Lourenço AB, dos Santos CAC. Energy, exergy, and exergoeconomic evaluations of a micro-trigeneration system. J Brazilian Soc Mech Sci Eng 2020;42(6). https://doi.org/10.1007/s40430-020-02399-y.